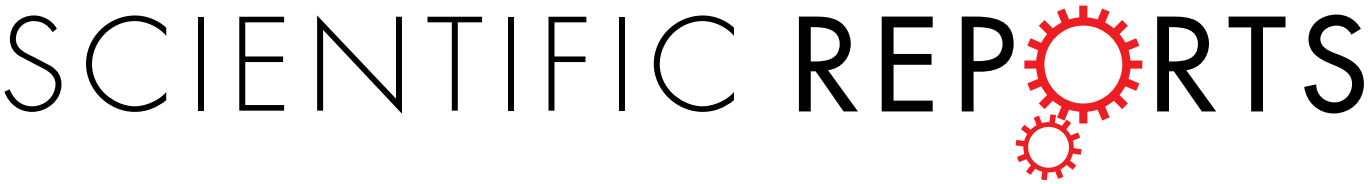

OPEN

Received: 09 December 2015
Accepted: 29 March 2016
Published: 20 April 2016

Ultrafast charge separation dynamics in opaque, operational dye-sensitized solar cells revealed by femtosecond diffuse reflectance spectroscopy

Elham Ghadiri[1,2], Shaik M. Zakeeruddin[3], Anders Hagfeldt[4], Michael Grätzel[3] & Jacques-E. Moser[1,2]

Efficient dye-sensitized solar cells are based on highly diffusive mesoscopic layers that render these devices opaque and unsuitable for ultrafast transient absorption spectroscopy measurements in transmission mode. We developed a novel sub-200 femtosecond time-resolved diffuse reflectance spectroscopy scheme combined with potentiostatic control to study various solar cells in fully operational condition. We studied performance optimized devices based on liquid redox electrolytes and opaque TiO_2 films, as well as other morphologies, such as TiO_2 fibers and nanotubes. Charge injection from the Z907 dye in all TiO_2 morphologies was observed to take place in the sub-200 fs time scale. The kinetics of electron-hole back recombination has features in the picosecond to nanosecond time scale. This observation is significantly different from what was reported in the literature where the electron-hole back recombination for transparent films of small particles is generally accepted to occur on a longer time scale of microseconds. The kinetics of the ultrafast electron injection remained unchanged for voltages between +500 mV and –690 mV, where the injection yield eventually drops steeply. The primary charge separation in Y123 organic dye based devices was clearly slower occurring in two picoseconds and no kinetic component on the shorter femtosecond time scale was recorded.

Dye-sensitized solar cells (DSCs) are promising candidates for solar energy conversion applications. These devices do not rely on rare or expensive materials, so they could be more cost-effective than cells based on silicon and thin-film technologies. Recently, DSCs device efficiency has reached a maximum power conversion efficiency of over 12% using donor- bridge - acceptor (D-π-A) zinc porphyrin dye in combination with a cobalt-based redox mediator[1].

The performance of DSCs is based on kinetics competition between the electron injection from the sensitizer to an electron collecting material, usually TiO_2, regeneration of the oxidized dye with redox electrolyte and unwanted back reactions of injected electrons recombining with oxidized dye molecules or oxidized species of redox electrolyte[2]. A challenge in this field is that the kinetics of charge carriers may be altered in complete devices showing top performances. A deep understanding of many parameters controlling the overall performance is crucial for achieving improvements in performance. Despite numerous studies, there is still a debate on the electron injection time scale for the optimized solar cells and according to the proposed "kinetics redundancy", the optimized solar cells might not have ultrafast electron injection kinetics[3]. Existing studies are mainly based on the classical pump-probe transient absorption spectroscopy, which is widely used to measure the kinetics of electron injection processes. Since optical transparency is required, to perform transient absorption studies, only

[1]Photochemical Dynamics Group , Ecole Polytechnique Fédérale de Lausanne, CH-1015 Lausanne, Switzerland. [2]Lausanne Centre for Ultrafast Science (LACUS), Ecole Polytechnique Fédérale de Lausanne, CH-1015 Lausanne, Switzerland. [3]Laboratory for Photonics and Interfaces, Ecole Polytechnique Fédérale de Lausanne, CH-1015 Lausanne, Switzerland. [4]Laboratory of Photomolecular Science, Ecole Polytechnique Fédérale de Lausanne, CH-1015 Lausanne, Switzerland. Correspondence and requests for materials should be addressed to E.G. (email: elham.ghadiri@alumni.epfl.ch)

model systems based on a transparent TiO_2 thin film sensitized with various dyes and semiconductors in different environments (solid samples or in solution) were investigated so far[3–7]. It should, however, be noted that the most efficient liquid-based solar cell devices are not transparent. Indeed, these devices are based on a double layer of TiO_2 film, which contains a scattering layer made of 400 nm TiO_2 particles deposited on top of a mesoporous transparent layer[8]. The resulting light transmittance of the cell is less than 15% in the visible region and, hence, conventional transient absorption spectroscopy in transmission mode cannot be applied in this case. Despite the importance of the subject, the kinetics of electron injection in actual optimized, opaque dye-sensitized solar cell devices under working conditions has not so far been reported.

We aim here to investigate the dynamics of charge carriers directly in fully functional devices, using potential control and state-of-the-art pump-probe diffuse reflectance spectroscopy. Despite the great potential of the latter technique, only a few studies can be found in literature investigating its implementation and application. We aim to demonstrate that diffuse reflectance spectroscopy is of great value for time-resolved analysis of photophysical processes in opaque or highly absorbing materials. Time-resolved diffuse reflectance spectroscopy was first reported by Wilkinson *et al.*[9] in microsecond time regime in 1981 followed by Bowman *et al.*[10] and Asahi *et al.*[11,12]. The technique was utilized on scattering systems like powders of organic microcrystals, and by Furube *et al.*[13] on DSCs under open circuit condition. Here we have developed an ultrafast time-resolved pump-probe diffuse reflectance spectrometer with a sub-200 femtoseconds time-resolution. This required application of novel optical design for the collection of diffuse reflected light. In addition and for the first time, we combined the femtosecond time-resolved diffuse reflectance laser spectroscopy with potential control and photovoltage measurements.

Furthermore, the technique has enabled us to investigate the charge separation kinetics in DSCs based on photoanodes of other TiO_2 film morphologies. For example, we studied samples of anodized nanotubes on Ti foil[14,15] and nanostructured fibers[16,17]. These samples have exhibited promising behavior in cell performance but are not optically transparent and are not suitable for investigation with pump-probe transmission based transient absorption technique.

Our studies reveal that the charge separation dynamics in Ru-based dye in the complete device is ultrafast and is indeed affected by the morphology of the TiO_2 film. We observed an early charge recombination in scattering TiO_2 particles, TiO_2 fibers and anodized TiO_2 nanotubes. These recombinations had different amplitudes and were not previously reported for small particles and are rationalized in terms of different electron mobility and trapping states in different TiO_2 films. Under an applied voltage bias condition from +500 mV up to –690 mV, the kinetics of the electron injection from the dye excited-state into the oxide remains ultrafast. However, the injection yield decreases at the bias point of –690 mV. In contrast to Ru-complex based dye, the organic D-π-A dye Y123 exhibited slower charge injection kinetics. The excited-state lifetime of Y123 dye is measured to be 50 ps. The time constant of the electron injection process is measured being 1.1 ps. While this classifies as ultrafast, it is about one order of magnitude slower than for Ru-based dyes, which was measured to have features in femtosecond time scale.

Results and Discussions

Figure 1a shows the schematics of the standard optimized high-performance liquid solar cell. In the conventional DSC scheme, the mesoporous layer is made of 20 nm-diameter interconnected TiO_2 particles. Although this structure offers a large surface area for dye adsorption, Rayleigh scattering with this size of TiO_2 particles is small, resulting in high transparency of the dye-sensitized film in a broad spectral region. A significant amount of light (70% in the near infrared region) is transmitted without interacting with dye molecules in the cell. The working electrode applied in highly efficient devices is based on a TiO_2 double layer film[18], sensitized with dye molecules on top of a $TiCl_4$-treated conductive glass. The structure of these samples is shown in Fig. 1a. The first layer is a transparent mesoporous anatase TiO_2 film, consisting of interconnected spherical nanoparticles (20 nm). Another layer made of 400 nm-diameter TiO_2 particles is deposited on top of the transparent layer. Figure 1b shows the total transmittance, total reflectance and total absorptance of the Z907 dye-sensitized TiO_2 double layer film based DSC photoanode. The 400 nm particles act as light scattering centers enhancing light absorption by increasing the light pathway within the film. Consequently, the total transmittance of the cell in the visible and near-infrared region is less than 15% as it can be seen in Fig. 1b. This suggests that the diffuse reflectance spectroscopy is the only versatile optical laser spectroscopy technique capable of studying such devices. The Kubelka-Munk function, F(R) spectra is derived from diffuse reflectance of the film according to equation (3), presented in the method section. The F(R) spectrum is compared with the absorptance spectrum of the opaque photoanode in Fig. 1b. As it is seen, the Kubelka-Munk spectrum follows the shape of the absorptance curve, and the similarity in both spectra is observed. The peak around 520 nm corresponds to the Z907 dye ground state absorption that serves as an absorbing medium. The shoulder at 380 nm corresponds to the absorption of TiO_2 substrate that serves as the scattering media in Kubelka-Munk theory.

Two types of liquid electrolyte-based devices were selected for the present study. The first type of DSC is prepared with a Ru-complex sensitizer (Z907) in combination with an iodide/ triiodide based redox electrolyte in 3-methoxypropionitrile solvent. This combination was reported to result in highly stable devices when subjected to light and thermal stress during long-term aging[19,20]. The second type of cell is based on the organic D-π-A, sensitizer Y123 and a cobalt complex-based redox electrolyte. This type of device yielded a power conversion efficiency of over 9%[21,22] and over 12% in combination with a porphyrin dye[1]. The thickness of both TiO_2 layers affects both photocurrent and photovoltage, which were optimized in earlier studies in terms of final power conversion efficiency[8].

Femtosecond diffuse reflectance spectroscopy on operational DSC device based on Z907 sensitizer. In order to unravel the electron injection dynamics in dye-sensitized opaque solar cells, we utilized pump-probe diffuse reflectance spectroscopy. We applied this technique to the study of Z907 dye-sensitized TiO_2

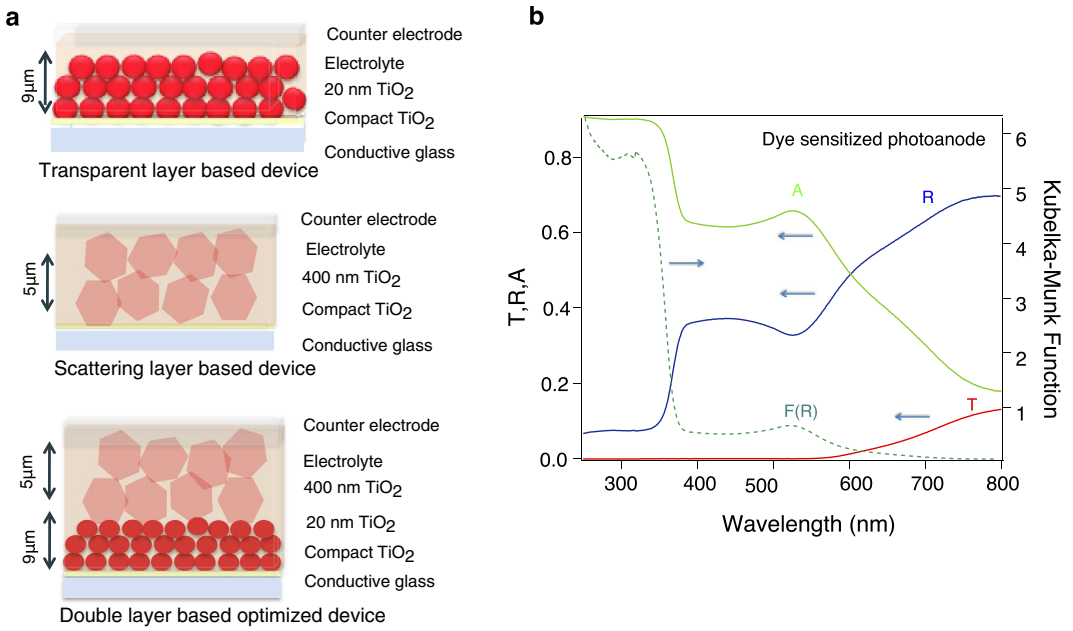

Figure 1. Device architecture and optical properties of complete photoanode. (**a**) Schematic of the optimized highly efficient liquid DSC based on single layer and double layer TiO_2 films. This represents examples of the devices that have been studied. (**b**) Steady-state optical parameters of a Z907 sensitized TiO_2 double layer photoanode applied in highly efficient DSC devices. Total transmittance (Red), diffuse reflectance (blue), absorptance (green) and Kubelka- Munk function (dashed green) are depicted. Kubelka-Munk function and absorptance are defined according to equations (1) and (3) depicted in the method section. The total transmittance of the cell in the visible and infrared region is less than 15%. The Kubelka-Munk function spectrum follows the shape of the absorptance spectrum.

films, which are from the same family of N719 and N3 Ru-based dyes. According to earlier transient absorption studies on N719 (cis-bis (isothiocyanate)bis(4,4′-dicarboxylic-2,2′-bipyridyl) ruthenium(II)) and N3 (cis-di(thiocyanate)bis(2,2′-bipyridyl-4,4′-dicarboxylic acid)ruthenium(II)) dye-sensitized TiO_2 films, the transient absorption spectrum around 800 nm is assigned to the oxidized dye molecules[13,23–25] and the absorption spectrum around 1200 nm is attributed to absorption by conduction band electrons[13,26,27]. The kinetics of electron injection in the complete device is studied by monitoring the evolution of oxidized dye molecules and photo-injected electrons in TiO_2. The oxidized dye molecules are monitored at the characteristic absorption onset in the visible wavelength region at 670 nm or in the NIR region at 840 nm, and photo-injected electrons are monitored at 1200 nm.

Figure 2a,b compare the early and later time evolution of absorptance of oxidized dye molecules anchored on three different TiO_2 films in the presence of MPN solvent. The samples are excited at 600 nm. The time delayed diffuse reflected probe beam is measured at 840 nm. Transient absorptance change is extracted from the measured transient diffuse reflectance change given by equation (2), depicted in the method section. In Fig. 2a,b, it is seen that in the presence of MPN solvent, the kinetics of electron injection in double layer film resembles that of transparent film made of small TiO_2 particles. All samples have an instrument response-limited transient absorptance onset within 200 fs and a slow rise of the signal with a time constant of 1.1 ps.

The first ultrafast response limited rise of the signal corresponds to the ultrafast electron injection from dye to TiO_2 conduction band. Ultrafast fluorescence studies performed by Chergui and coworkers[28] on N719 sensitized TiO_2 small particles films revealed that the electron injection occurs with a time constant of 10 fs for non-thermalized levels of the dye and 120 fs from the thermalized level. The second slow rise component up to 5 ps is observed in all three TiO_2 films was also previously reported in measurements of transparent films by different research groups[29,30]. Studies by Wenger *et al.*[29] assigned this feature to the presence of dye aggregates in the films, which have a larger distance for electron injection and, therefore, less electronic coupling for electron transfer process. Sundström *et al.* proposed another description in terms of a two-state mechanism. They assigned the fast and slow components to the injection from the singlet and the triplet excited-states of the ruthenium complex, respectively[30].

Figure 2c illustrates the long time kinetics of the evolution of oxidized dye molecules up to 500 ps after excitation in the working cell based on TiO_2 double layer film. Remarkably, the kinetics features a decay component in several hundred picoseconds after excitation. The trace is fitted by an exponential decay function with a time constant of 4 ns. It should be noted that all measurements shown in Fig. 2 are performed at very low excitation intensities. For measurements shown in Fig. 2, the excitation energy of each pulse at the sample is 200 nJ. The repetition rate is 0.5 kHz. The beam diameter is close to 500 µm. Under these conditions, the excitation irradiance is 102 µJ cm^{-2}. With having the repetition rate of 0.5 kHz, the excitation power is 51 mW cm^{-2}, which is equivalent to 50% of the sun irradiance power at AM 1.5 condition. In addition, the number of photons normalized to the volume of TiO_2 within the irradiation area is about 2.15×10^{11}. This is significantly smaller than the number of adsorbed dye

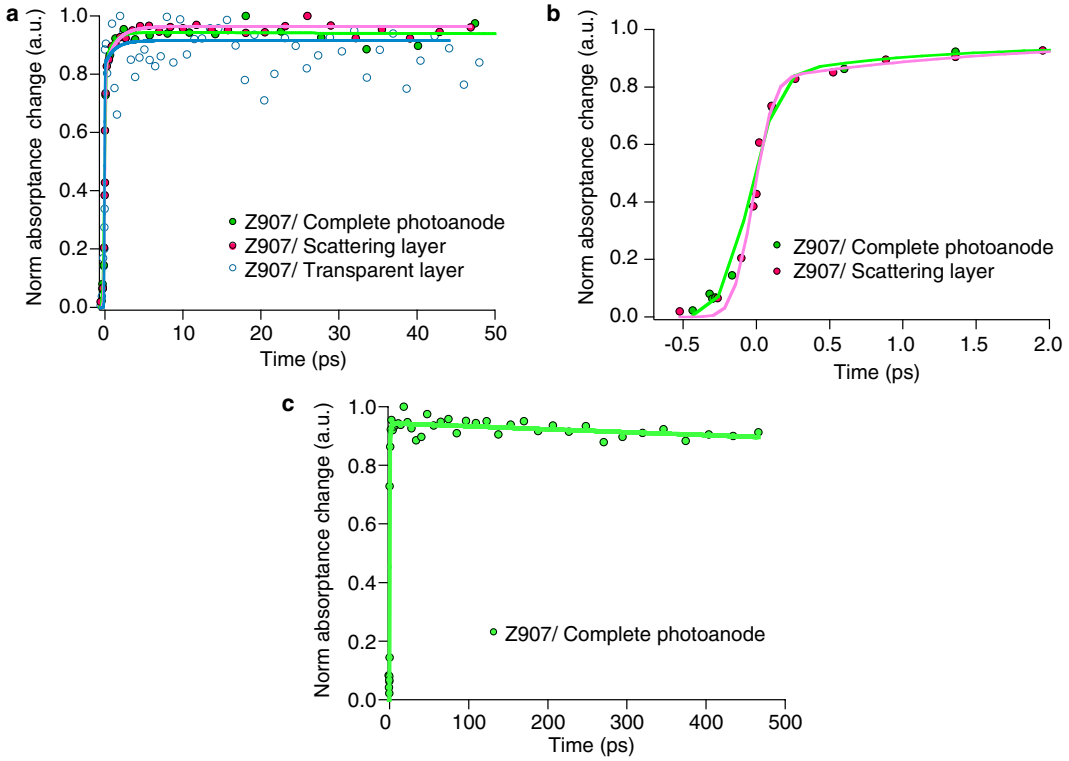

Figure 2. Transient diffuse reflectance of dye-sensitized TiO_2 photoanodes. Samples are covered with MPN solvent. $\lambda_{ex} = 600$ nm and $\lambda_{obs} = 850$ nm. (**a**) Evolution of Z907 oxidized dye molecule anchored on transparent film (blue markers), scattering film (red marker) and double layer film (green marker) recorded up to 50 ps after excitation. Lines are fitted to convoluted exponential function. (**b**) Kinetics of oxidized dye molecule anchored on scattering film (red) and complete photoanode (green) up to 2 ps after excitation. Fitting parameters for complete photoanode are $A = 0.11$, $\tau_1 = 1.08$ ps, $\sigma = 0.158$ ps and $\mu = -0.05$ ps. Fitting parameters for scattering layer are $A = 0.15$, $\tau_1 = 1.75$ ps, $\sigma = 0.109$ ps and $\mu = -0.024$ ps. (**c**) Kinetics of oxidized dye molecule in full photoanode until 500 ps after excitation. Fitting parameters are $A = 0.1$, $\tau_1 = 1.18$ ps, $\sigma = 0.164$ ps, $\mu = -0.05$ ps, $B = 0.9$ and $\tau_2 = 4$ ns. A and B are the pre-exponential factors and τ is the time constant. σ and μ are the broadening and zero onset of Gaussian function fit to cross-correlation of the pump and probe.

molecules on the microscopic surface of TiO_2 film, within the irradiated area which is 9.8×10^{16} (assuming one monolayer of adsorbed dye molecules). Hence, our observations are not due to some non-linear effects.

The excitation intensity dependence of the observed kinetics is also presented in Supplementary information, Figure S4. All traces measured at low excitation intensities can be fitted by a single exponential function. This early decay kinetics is again observed when the evolution of oxidized dye molecules is monitored in the visible wavelength region at 670 nm (Supplementary Figure S5). Moreover, the same depleting kinetics can be observed (Fig. 3b) when photo-injected electrons are monitored at 1200 nm in the presence of the electrolyte. Therefore, we assign the early decay kinetics observed for the complete opaque DSC in the presence of MPN solvent, to the early back recombination of photo-injected electrons with oxidized dye molecules.

The kinetics of back recombination is even more strongly accelerated in the presence of the electrolyte. Traces in Fig. 3a compare the measurements in the presence (black markers) and absence of redox electrolyte (red markers) on double layer TiO_2 film. In the vicinity of the redox electrolyte, the formation of the signal is again ultrafast, and the sub-200 fs ultrafast component is still present. As it can be observed, 26% of the signal of the oxidized dye molecule decays with a time constant of $\tau_1 = 9$ ps. The same fast decay kinetics are also present in the samples dipped in the redox-inactive ionic liquid, 3-methyl-1-ethylimidazolium bis (trifluoromethane) sulfonimide (EMITFSI), (see Fig. 4d). Therefore, the observed kinetics cannot be assigned to processes like reductive quenching of the excited-state of the dye molecules by redox electrolyte. The accelerated charge recombination in the presence of both redox active and redox inactive electrolyte in some picoseconds after excitation is rationalized by electric fields induced by the charges in the electrolyte and charge screening effects. The local electric field induced by ions present in the redox electrolyte or ionic liquid at the surface is accelerating the charge recombination between electron-hole geminate pair after initial charge separation.

Figure 3b provides more evidence, as photo-injected electrons in TiO_2 are directly monitored at 1200 nm. The trace is fitted with two exponential decay functions. The rate constant of the fast decay component of photoelectrons measured at 1200 nm is $1.1 \times 10^{11}\ s^{-1}$ and for the slower decay kinetic is $5.917 \times 10^{8}\ s^{-1}$, giving a lifetime of 8.9 ps and 1.7 ns, respectively. Interestingly, these time constants are consistent with the kinetics fit values of measurements at 840 nm monitoring oxidized dye molecules. Taken together, the observed decay kinetics at 840 nm

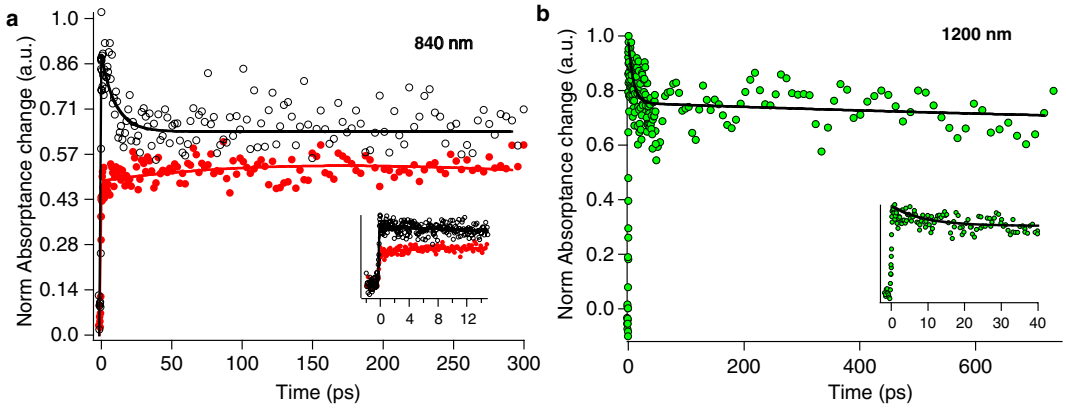

Figure 3. Transient absorptance on complete device. Normalized transient absorptance deduced from femtosecond diffuse reflectance measurements on a DSC composed of Z907 dye-sensitized TiO_2 double layer. (**a**) Probed at 840 nm monitoring the kinetics of oxidized dye molecules in the presence of MPN solvent (red markers) and Iodide based electrolyte Z946 (black markers); the solid lines correspond the fit to the result by a two exponential function. The inset shows the short delay time scan of the observed kinetics at 840 nm in the presence of MPN solvent and electrolyte. (**b**) The observed kinetics in the vicinity of electrolyte measured at 1200 nm monitoring the kinetics of photo-injected electrons in TiO_2. The solid lines correspond the fit to the result by exponential function. The time constant of exponential fit to the measurements at 840 nm is $\tau_1 = 9.22$ ps and for trace measured at 1200 nm is $\tau_1 = 8.9$ ps. The pump wavelength is 530 nm and pulse intensity is 200 nJ.

and the mirror kinetics at 1200 nm are due to an early back recombination of photo-injected electrons with the oxidized dye molecules anchored on the surface of TiO_2 particles.

Therefore, a significant observation in our measurements of the DSC devices based on scattering particles and all other TiO_2 morphologies (as it is discussed below), is that the kinetics of electron back recombination with oxidized dye molecule has features in the picosecond to nanosecond time scale. This observation is remarkably different to what is normally stated in the literature for model systems of transparent films made of small particles. The small particles based films are the only morphology that has been studied to date. In earlier studies of small TiO_2 particles sensitized with Ru dyes based on transient absorption spectroscopy at visible or NIR region or by 2D-IR spectroscopy[23,31–33], such electron back recombination was not observed and the oxidized dye molecule was accepted to be stable until much longer time scale of microseconds. We observe that the kinetics is accelerated in full device relative to what is so far accepted for small particles. In a complementary study, presented in Supplementary Table S1, the photovoltaic, optical and structural characteristics of the transparent and double layer based devices are depicted. The value of photocurrent normalized to the light absorptance of the scattering layer is about 30% less than that for transparent layer based device. This indicates that in big particles some fraction of photoelectrons are lost and is consistent with the early back recombination of electrons and oxidized dye molecules observed in laser spectroscopy measurements.

In addition, the pump-probe diffuse reflectance technique has also enabled us to investigate the electron injection profiles in many other DSC devices. These studies include measurements of different opaque nanostructured TiO_2 films such as TiO_2 nanofibers[16] and TiO_2 nanotubes. TiO_2 nanotubes are prepared by anodization of Ti foil as the substrate[14]. Due to opacity, these samples could never be studied by transmission based transient absorption technique.

Figure 4 shows the dynamics of electron injection on Z907 dye-sensitized TiO_2 films of different morphologies monitored at 840 nm. Panel a shows the kinetics of charge separation in Z907 dye-sensitized standard double layer based DSC device in the presence and absence of redox electrolyte. Panel b depicts the pump-probe diffuse reflectance measurements on Z907 dye-sensitized anodized TiO_2 nanotube film on Ti foil. The same studies are performed on dye-sensitized TiO_2 nanostructured fibers. Measurements of fibers in the presence of cobalt-based electrolyte (CO^{II}/CO^{III}) and also redox-inactive electrolyte (EMITFSI), are shown in panel c and d, respectively. It is interesting that in all measurements the electron injection is still in the ultrafast regime and recombination features with different amplitudes comparable to that of double layer film is present. In standard full DSC based on double layer film 30% of the signal decays in 20 ps after excitation, this compares to only 16% for DSCs based on anodized nanotubes.

The observed kinetics in the presence of redox-inactive ionic liquid suggests that the decay kinetics cannot be due to the reductive quenching of the dye excited-state by redox electrolyte. The observed difference in early back recombination of photoelectrons in the TiO_2 films of nanoparticles and anodized nanotubes is rationalized in terms of morphological parameters of the two films such as trap state distribution.

We hypothesize that photo-injected electrons may get trapped in the TiO_2 particle surface states where they form geminate pairs with holes (oxidized dye molecules) and result in the observed early fast recombination in different TiO_2 morphologies with different amplitudes. It should be noted that, our control studies (Figure S3) shows that at low excitation intensities of 0.25 sun irradiance at AM1.5, the excited dyes inject more than $3.8 \times 10^{16}\,cm^{-3}$ electrons into the TiO_2, which is much smaller than the trap state density ($10^{18}\,cm^{-3}$ to $10^{20}\,cm^{-3}$)

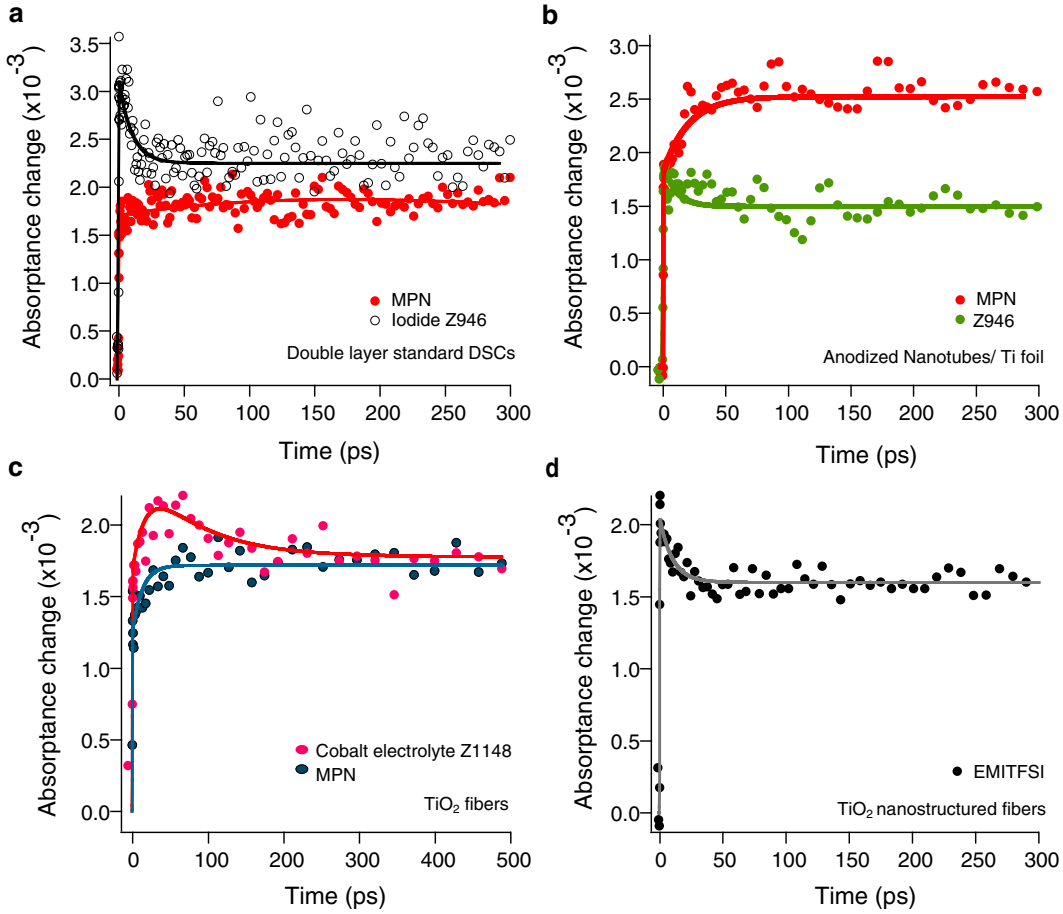

Figure 4. Transient absorptance on different nanostructured opaque TiO_2 films based devices. Transient absorptance change deduced from transient diffuse reflectance measurements on DSCs based on different TiO_2 opaque films. $\lambda_{ex} = 530$ nm and $\lambda_{obs} = 840$ nm. (**a**) Standard DSC based on TiO_2 double layer dipped in MPN solvent (red) and iodide-based redox electrolyte (black). 30% of the signal decays in 20 ps in the vicinity of electrolyte. (**b**) DSC based on anodized TiO_2 nanotubes on Ti foil dipped in MPN solvent (red) and iodide-based redox electrolyte (green). 16% of the signal decays in 20 ps after excitation in the vicinity of the electrolyte. (**c**) DSC based on TiO_2 fibers in MPN solvent (blue) and cobalt-based redox electrolyte (pink). In the presence of cobalt electrolyte, 20% of signal decays in 200 ps after excitation. (**d**) DSC based on TiO_2 fibers dipped in redox-inactive ionic liquid, EMITFSI (black), 28% of the signal decays in 20 ps after excitation. The measurements are performed at the same excitation intensities.

reported for TiO_2 films[14]. One should also consider the energetic distribution of these traps. For instance, the trap state distribution in the anodized nanotubes is measured using macroscopic techniques like charge extraction experiments by Hagfeldt *et al.*[14]. The nanotubular electrodes have a trap state distribution significantly different from nanoparticulate electrodes. Nanotubes possess relatively deeper traps with a characteristic energy of the exponential distribution more than twice than that of nanoparticulate electrodes. Throughout time-resolved terahertz studies, Schmuttenmaer *et al.*[34] have claimed that the low mobility in polycrystalline TiO_2 nanotubes is not only due to scattering from grain boundaries or disorders as is in other nanomaterials but instead results from a single sharp resonance from exciton-like trap states. These observations are in good agreement with our spectroscopy studies. Indeed, electrons can get more localized in energetically deeper traps in nanotubes films and, therefore, less early back recombination with oxidized dye molecule is observed in these films in comparison with nanoparticles based films.

Our observations show direct evidence of an ultrafast electron injection occurring in a complete Ru-dye based DSC device. This has not been confirmed so far for DSCs having all components like scattering layer, electrolyte, conductive glass, etc. Charge injection from the amphiphilic Ru^{II}(bipyridyl) Z907 dye in all different TiO_2 morphologies was observed to take place in the sub-200 fs time scale. We observed that the kinetics of charge separation is indeed influenced by the morphological parameters of the TiO_2 substrate. The photo-injected electron in TiO_2 fibers, nanotubes, and 400 nm particles shows prompt back recombination kinetics with oxidized dye molecules in the picoseconds-nanoseconds time scale after excitation. Electronic parameters like density of trap states and energetic of trapped electrons, i.e. how deep electrons are trapped, and consequently the mobility of electrons, might play a vital role in the behavior of photo-injected electrons after initial interfacial charge separation.

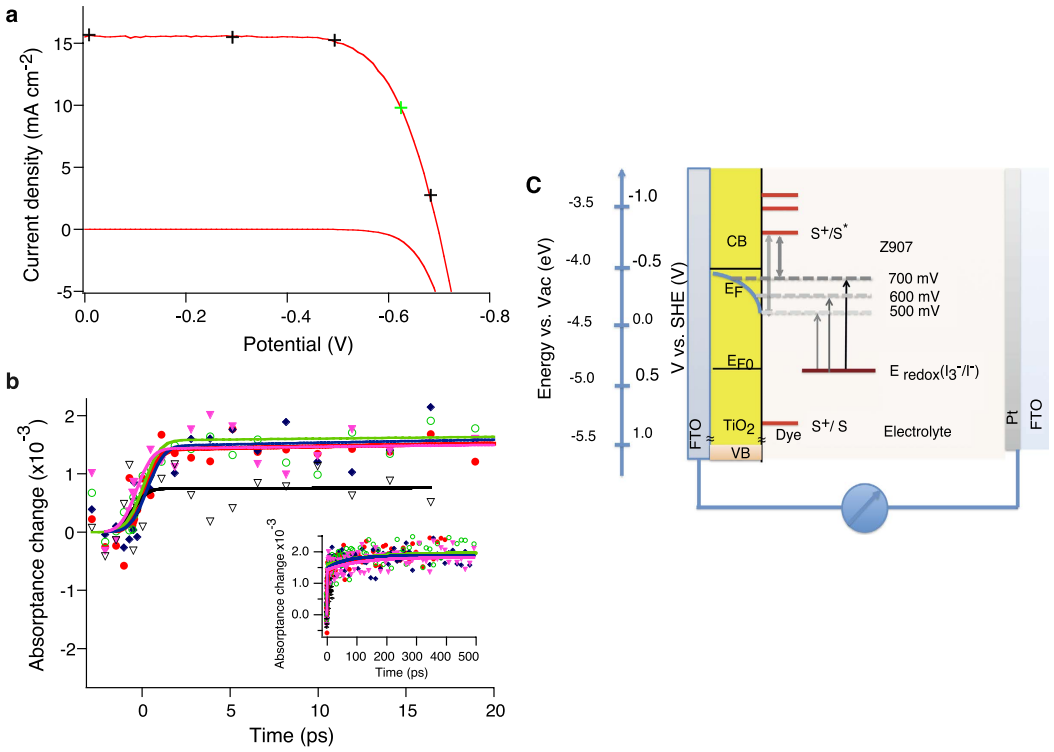

Figure 5. J-V analysis, pump-probe diffuse reflectance spectroscopy, and energy level diagram of the full device. (**a**) The J-V characteristics of an optimized standard DSC device based on Z907 dye and Z946 electrolyte measured in dark and under irradiance of AM 1.5G sunlight of 100 mW cm^{-2}. (**b**) diffuse reflectance measurements on DSC under apply bias voltage. Signals are recorded at 840 nm reflecting the kinetic of oxidized dye molecules, Green circle: short circuit, Red circle: −500 mV, blue diamond: +500 mV, pink triangle: −320 mV, black triangle: −690 mV. (**c**) Energy level diagram of complete DSC. The energy level of quasi-Fermi level E_{fn} at the bias voltage of 300 mV and 700 mV are depicted. Trap state density exponentially increases with increasing the energy level. The E_{fn} level respect to E_{f0} at 3 different biases is illustrated. Trap density at voltage difference of 500 meV, 600 meV and 700 meV is approximately respectively 1×10^{19}, 2×10^{19} and 7×10^{19} cm^{-3}. Arrows show the shift in the quasi-Fermi level position and the energy difference of quasi-Fermi level and dye LUMO level.

We have combined the diffuse reflectance spectroscopy with potentiometric techniques to monitor the electron injection process in DSC standard device under working condition. Figure 5a shows the photovoltaic characteristics of the Z907 sensitizer and iodide based redox electrolyte device. The photovoltaic parameters of the device at full sunlight are; short circuit current density (Jsc) of 15.5 mA/cm^2, open circuit photovoltage (Voc) of 698 mV, fill factor (FF) of 0.71 and power conversion efficiency (PCE) of 7.6%. Figure 5b presents the typical transient absorptance of the cell in short circuit condition and under different bias voltages of +500 mV, −500 mV (close to max power point) and −690 mV. Transient absorptance traces are not easily distinguishable. All traces in this figure can be fitted by exponential function with close fitting parameters; a component with a lifetime of 50–70 ps, and the flat behavior until hundred picoseconds, which is shown in inset. By raising the bias to −690 mV close to open circuit condition, the amplitude of the observed signal is almost half of the others while the kinetics remain similar. In other words, as the amplitude of the pump-probe signal is proportional to the number of oxidized dye molecules, with increasing the applied bias voltage the quantum yield of electron injection is reduced. The energy level diagram, which contains the energy level of the conduction band of TiO_2 (CB), HOMO and LUMO level of Z907 dye and iodide-based redox electrolyte (Eredox) and trap state distribution are illustrated in Fig. 5c. Increasing the forward bias voltage would raise the quasi-Fermi level position by filling up the trap states to some extent in TiO_2, which is highlighted in Fig. 5c. As it is observed by shifting the quasi-Fermi level toward the LUMO level of the dye, the energy difference gets noticeably smaller. In example the energy difference at the bias level of −600 mV is 75% of the energy difference at the bias level of −500 mV and further reduces to 50% at a higher bias level of −700 mV.

It should be noted that at the bias level of −690 mV, the amount of voltage in the films is less than this value due to the dark current. The voltage drop in the cell at a voltage bias of −700 mV is estimated as 90 mV. By taking account of this voltage drop, the respective amount of the cell photocurrent measured at bias voltages up to −500 mV and at −690 mV is consistent with the respective amplitude of the pump-probe signals. In our control studies (Supplementary Figures S6 and S7), the photovoltage induced by each laser pulse is estimated to be only of μV order when the cell is biased in the conventional voltages of hundreds of mV. This indicates that our pump-probe measurements under potentiostatic condition can be considered as a perturbation technique.

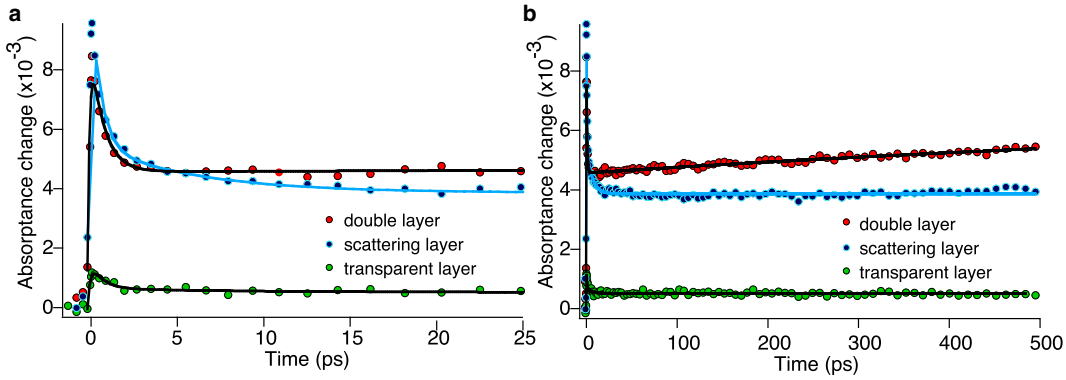

Figure 6. Femtosecond diffuse reflectance measurements on DSC devices based on organic D- π-A dye, Y123. Measurements are in the presence of cobalt-based redox mediator, Z1148 electrolyte. Red and blue markers are the measurements on the double layer and scattering layer films respectively and trace with green markers correspond to the transparent layer. Pump wavelength is 600 nm, and the probe wavelength is 840 nm. (**a**) The kinetics is drawn until 25 ps after excitation. In all three TiO_2 films, the amplitude of the signal decays to half of its value in short time scale after excitation. (**b**) The kinetics are drawn until 500 ps after excitation. Solid lines are the result of fitting two exponential functions to the data.

Electron injection in DSC based on D-π-A organic sensitizer and cobalt electrolyte. One of the most significant advances in design of light-harvesting materials is the so-called donor-conjugated linker-acceptor (D-π-A) organic dyes. In comparison with Ru-based dyes, organic dyes have higher molar extinction coefficient and can be readily designed for a desired absorption spectrum[1,35–37]. These molecular structures look attractive in terms of electron donor-acceptor interactions[35]. In order to understand the electron injection dynamics in these systems, femtosecond diffuse reflectance spectroscopy is applied to DSC devices containing Y123 and a cobalt complex based redox electrolyte. Three different morphologies of the photoanode are used, and the results are compared in Fig. 6. In these measurements, the pump beam wavelength is 600 nm to excite the dye, and the probe beam is 840 nm. Upon laser excitation, an ultrafast formation of the signal happens in 200 fs, followed by a fast decay of the signal to 50% of its amplitude in 2 ps. After two picoseconds, the signal reaches a plateau in all the 3 morphologies of the TiO_2 layers. Unlike Ru-based dyes, no obvious difference is observed in the kinetics for measurements in the presence of MPN solvent and redox electrolyte and the medium has no influence on the observed kinetics (measurements in the presence of MPN solvent are provided in Supplementary information Figure S9). The slow growth component of the signal in hundred picoseconds time scale seen in the films made of scattering particles or the double layer film, is assigned to the electron injection from dye aggregates. This component is removed from the signal when the sample is immersed in acetonitrile solvent for several hours (Supplementary Figure S10). TiO_2 films prepared with scattering particles might have enough space to accommodate aggregated dye molecules within the pores, which are loosely in contact with the TiO_2 layer. This makes a larger distance for electron transfer between the dye and TiO_2.

In order to study the mechanism of the very fast decay of the signal in 2 ps, we performed the transient broadband absorption measurements. We compared the broadband transient absorption of Y123-sensitized TiO_2 film with that of Y123 dye in solution as a reference sample where interfacial electron transfer process is deactivated. By comparison of the recorded spectra of the dye-sensitized films with the dye in solution we can clearly resolve the spectral absorption contribution of the excited-state and oxidized state of the Y123 dye. The transient absorption spectra of the samples measured at NIR region is also shown in Supplementary Figure S11. The ground state optical absorption spectrum of the dye is provided in Supplementary Figure S8. For the dye in solution (Fig. 7a), the negative peak at the characteristic ground state absorption of the dye around 520 nm, is attributed to the ground state bleaching of the dye formed upon photo-excitation. In Fig. 7a, a positive transient absorption is observed in the wavelength region from 630 nm up to 700 nm. This transition is assigned to excited-state absorption of dye molecule. The dye excited-state relaxation time constant is 52 ps and has a mirror-like kinetics to ground state relaxation. The transient absorbance spectrum of the dye-sensitized TiO_2 films is presented in Fig. 7b. In this sample, the ground state bleaching is observed at 580 nm, which is around 60 nm shifted with respect to the steady-state absorption onset of the dye.

This red-shift in the transient absorption spectrum is an evidence of a Stark-shift of the absorption spectrum of the dye molecule. The Stark-shift is explained by the shift of ground state absorption of the dye molecule due to the local electric field induced by the electric dipole of the neighbor dye molecules. This effect was also previously reported for the same family of D-π-A dyes[36,37]. For the dye-sensitized TiO_2 film the positive absorption feature is extended over the 630 nm wavelength regions. This positive feature is now assigned to a contribution of both of the excited-state absorption of the dye and the absorption by oxidized dye molecule formed upon injection of electrons into TiO_2 conduction band.

Figure 8 compares the kinetics of a Y123 sensitized TiO_2 film probed in two different wavelength regions of 690 nm and 740 nm. According to Fig. 7a, at 690 nm the excited-state of Y123 has absorption while at 740 nm the excited-state does not absorb. Therefore, the blue trace in Fig. 8 recorded at 740 nm, represents a pure monitoring of the kinetics of the electron injection process. The formation of the signal, which reflects the electron injection

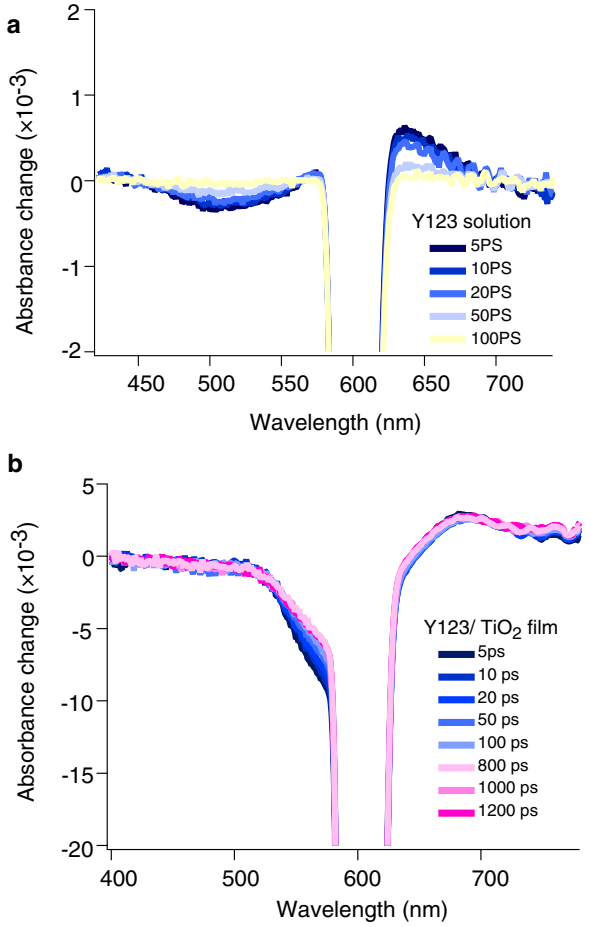

Figure 7. Transient white light continuum absorbance spectrum. (**a**) Y123 dye measured in solution and (**b**) Y123 sensitized TiO_2 transparent film, in the visible light wavelength region. Excitation intensities are 300 nJ/ pulse for films and 1000 nJ/pulse for measurement in solution. Measurements in solution are performed under N_2 bubbling.

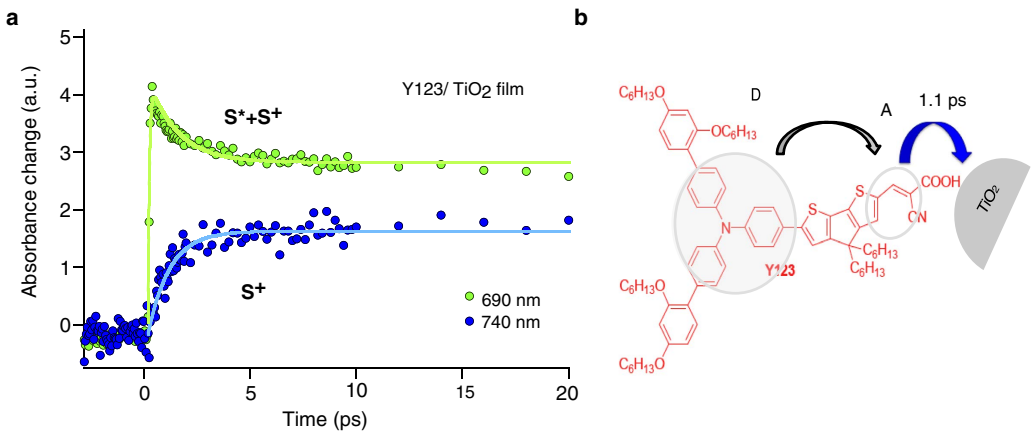

Figure 8. Comparison of the kinetics observed in the Y123 sensitized TiO_2 film at different wavelength regions of 690 nm and 740 nm and Y123 molecular structure. (**a**) Transient absorptance of Y123 sensitized TiO_2 films at 690 nm (green) and 740 nm (blue). The formation of the blue trace measured at 740 nm, which reflects the electron injection time, is occurring in picosecond time scale and is fitted with an exponential growth function with a time constant of 1.1 ps. (**b**) Y123 molecular structure and schematic of electron transfer processes. Blue arrow shows the electron injection process.

time, is occurring in picosecond time scale and is fitted with an exponential growth function with a time constant of 1.1 ps. As a result, we observe that in the Y123 D-π-A dye, the charge injection kinetics is not as fast as in Ru-based dyes, as reported by Chergui and co-workers[28].

The difference in the electron injection time in the Y123 with Ru-based dyes should be due to the D-π-A structure of this dye and its coupling with the TiO_2 film. In the Y123 dye, the electron donor part is the triphenylamine unit, and the acceptor orbitals are located on the cyanoacrylate group. Cyclopentadithienophene (CPDT) is working as a π-bridge between the donor and acceptor parts for the conjugation of electrons. This bridge helps increasing the dipole moment and enhancement in the molar extinction coefficient of the dye molecule[38]. Our results suggest that the relaxation of the excited-state is fast with a time constant of 52 ps. This process competes with electron injection into the lower lying conduction band of TiO_2. Moreover, non-adiabatic charge transfer from a molecular electronic excited state into a continuum of acceptor levels constituted by the conduction band of a semiconductor can be described by Fermi's golden rule[2]. Due to the very high density of acceptor levels, the nuclear factor in the equation tends to a constant value. As a consequence, the thermodynamics of the process, the temperature, and the reorganization energy are not expected to affect the injection dynamics. The electronic coupling between the donor and the acceptor (electronic coupling matrix element squared $|H|^2$) is then likely to control in a large extend the electron transfer rate. As $|H|^2$ depends exponentially upon the charge transfer distance, the adsorption geometry and the electronic coupling between the dye's HOMO and the empty d^4 orbital manifold of Ti^{IV} sites on which the dye is anchored must be determining the electron injection time.

In summary, our experimental technique allowed us to reveal the charge separation dynamics in a complete opaque solar cell device under applied bias voltage. Also, the interfacial charge separation in different dye-sensitized opaque TiO_2 nanostructured interfaces was determined. We showed that this technique could be a powerful and sensitive tool for measurements of opaque and highly absorbing materials. Coupling diffuse reflectance spectroscopy with potentiometric characterization tools gives a unique possibility to study charge carriers in devices under real operational conditions. In Ru-complex based solar cells, the kinetics of electron injection is confirmed to be ultrafast and is not affected by the bias voltage. In standard opaque and other TiO_2 morphologies based devices, after ultrafast electron injection, an early recombination of photo-injected electrons with oxidized dye molecules is observed with features in the picosecond to nanosecond time scale. The respective amplitude of this recombination process is influenced by morphological parameter i.e. trap states in TiO_2 films. We found that the ultrafast electron injection kinetics is not influenced by trap state filling upon increasing forward bias up to −500 mV. By applying a higher voltage close to open circuit conditions, and shifting the Fermi level of TiO_2 closer to the dye excited-state level, the electron injection is less efficient but the injection kinetics is still ultrafast. For a DSC with a Y123 organic dye, the dynamic of the excited-state of the dye and the kinetics of electron injection process significantly differ from Ru-base dyes. The excited-state relaxation in the Y123 dye molecule competes with electron injection into TiO_2. In contrast to Ru-complex based dyes, which show ultrafast electron injection in femtoseconds time scale, the electron injection for the Y123 dye is precisely monitored to occur within 2 ps after excitation of the dye.

Finally, the technique proposed here will be an excellent tool to be implemented for studies on highly absorbing materials, such as the new emerging perovskite based devices and can open up a new avenue of characterization research.

Methods

Pump-probe femtosecond diffuse reflectance spectrometer. In principle, the configuration of the diffuse reflectance spectroscopy is similar to the traditional transient absorption in transmission mode. The differences are: firstly in the probe beam geometry to collect the diffuse reflected light, which carries the information of transient species, secondly the sample structure and thirdly the optical model in data treatment. Here, a new optical scheme for collection of diffuse reflected light is designed which gives a unique time-resolution of sub-200 fs (Supplementary Figure S1). In this configuration, diffuse scattered light from the sample is collected, collimated, and focused onto the detector with two coupled off-axis 90° parabolic mirrors. Having this configuration, the large solid angle of light collection results in improved signal to noise ratio. The other advantage of using parabolic mirrors over lenses is that no further dispersion is introduced to the pulses; therefore, a better time-resolution is expected. Indeed, in this configuration, the time-resolution is limited by the time broadening of the beam in the diffusive sample. This time broadening is typically measured as about 30 fs in our samples[39]. For the transient absorption measurements, the pump beam at a defined wavelength is produced using a two-stage non-collinearly phase-matched optical parametric amplifier (NOPA). It is modulated using a synchronized chopper at a frequency of 0.5 kHz, which is half the repetition frequency of the laser. It is focused onto the sample at an angle of about 60° from normal. The pump beam has a diameter of 500 μm at the surface of the sample and typical energy of about 100–200 nJ/pulse. The probe beam is provided by a second NOPA having less energy than the pump on the sample to avoid multiple excitations and is focused having the spot size of around half of that of the pump. The polarization between the pump and probe beams is at the magic angle (54.7°). The transient response of the sample is measured by collecting the diffuse reflected pulses of the probe. The light scattered by the sample is focused onto the detector (photodiode: Nirvana detector, New Focus, model 2007). The signal of the detector is amplified by use of a lock-in amplifier. Lock-in parameters are set as integration time 1s, dwell time 4s, time constant 1s for measurements. A power supply (Weir) is used to apply a fixed bias voltage on the solar cell for diffuse reflectance measurements on the cell under voltage bias condition. The bias voltage between the two electrodes is changed from −690 mV to +500 mV and time-resolved diffuse reflectance of the device is measured at each applied bias. In these measurements, the pump and probe beam are irradiated to the cell from the backside (photoanode side), similar to the photovoltaic measurements. All the rest experimental details of experiments are similar to that previously explained.

Time-resolution of diffuse reflectance setup and linearity tests. The time-resolution of the setup is defined by using optical Kerr gating technique. In this technique pump and probe beams are focused and spatially overlapped on a non-linear media (SF10 crystal or glass substrate). The cross-correlation of pump and probe beam on a Kerr-media is measured at an angle of 45° between the polarization of pump and probe. We performed the cross-correlation experiment in the diffuse reflectance mode. As the Kerr- media once the SF10 crystal and another time the scattering sample with cover glass is used. The reason is to compare the broadening of the cross-correlation peak when the diffuse reflectance is measured on these types of substrates. The time-resolution of the setup is sub- 200 fs. It should be noted that the time-resolution of this technique is limited by the time broadening of the beam in the sample due to the scattering effect. This time broadening is measured to be 120 fs for our samples. This is in contrast with the transmission based transient absorption technique in which the time-resolution is solely determined by the pulse duration of pump and probe and their cross-correlation. The setup has an unprecedented sensitivity as it enables measurements of transparent, non-reflective samples (see green curve in Fig. 6) with a reasonable signal to noise ratio. In order to check the linearity of measurements, the intensity of the pump beam is changed over a broad range of energy from 0.047 μJ/pulse to a high intensity of 0.950 μJ/pulse. The diffuse reflectance of dye-sensitized sample at a fixed time delay (i.e. 50 ps) is measured. Both absorptance and Kubelka-Munk formalism show a very good linear fit to the measurements over the whole intensities of excitations (Supplementary Figures S2 and S3).

Data acquisition and treatment. In the configuration of reflectance measurements, the transient absorptance ($\mathcal{A}$) change can be measured and corrected by determining the absolute amount of diffuse reflected light with and without pump beam. This is practically achieved by chopping the pump pulse at half repetition frequency of the laser. The time-resolved diffuse reflectance of samples is measured by varying the delay time between the pump and probe pulses. Therefore, transient absorptance is displayed as:

$$\mathcal{A} = 1 - T - R \tag{1}$$

In case of opaque samples that the optical transmittance of sample is negligible, absorptance change ($\Delta\mathcal{A}$) can be deduced only from reflectance change, as:

$$\Delta\mathcal{A} = 1 - \frac{R}{R_0} = 1 - \frac{\Delta R + R_0}{R_0} \tag{2}$$

Where T is the intensity of the transmitted light and R and R_0 represent the intensity of the diffuse reflectance of probe pulse with and without excitation, respectively. The linearity of absorptance change upon excitation intensity is tested in our control studies, over a wide range of excitation intensities.

Another theory describing the optical behavior for a tightly packed isotropic absorbing and scattering medium is Kubelka-Munk[40,41], in which the Kubelka-Munk function relates the measurable so–called diffuse reflectance of the sample to the ratio of the absorption coefficient (K) and scattering coefficient (S). In the case of diluted medium, K is linearly dependent on concentration of absorbing species (c), in the same way, the Lambert-Beer Law is also valid in solutions; equation (3):

$$F(R_\infty) = \frac{K}{S} = \frac{(1 - R_\infty)^2}{2R} = \varepsilon c \frac{\ln(10)}{S} \tag{3}$$

For quantitative simulation, use of the Kubelka-Munk function is essential, however, treating the transient reflectance of the samples with both equations of (2) and (3), does not change the kinetics.

Broadband transient absorption setup. The pump−probe technique uses a compact CPA-2001, 1 kHz, Ti: Sapphire-amplified femtosecond laser (Clark-MXR), with a pulse width of about 120 fs at a wavelength of 775 nm. The pumping beam is generated using an NOPA tuned to 600 nm to generate pulses of approximately 8 μJ, that are then compressed in an SF10-glass prism pair down to duration of less than 60 fs (at FWHM). At the sample, the excitation pulse energy is decreased to a few hundred nJ. The probe beam is a white light continuum generated in a sapphire plate and splits before the sample into signals and reference beams in order to account for intensity fluctuations. Both beams were recorded shot by shot with a pair of 163 mm spectrographs (Andor Technology, SR163) equipped with 512 × 58 pixels back-thinned CCD cameras (Hamamatsu S07030-0906). The polarization of pump and probe pulses was set at a magic angle.

Solar cell fabrication. Dye-sensitized solar cells were fabricated using a double-layered photoanode made of mesoporous TiO_2 film. A transparent, 9 μm- thick layer of 20 nm particles was screen-printed onto an FTO glass plate (NSG-10, Nippon Sheet Glass). Subsequently, a 5 μm- thick layer of scattering particles (400 nm diameter) was deposited by screen-printing. The surface area of TiO_2 film was 1 cm^2. The TiO_2 film was sintered up to 500 °C by a stepwise heating program. Prior and after TiO_2 deposition a $TiCl_4$ treatment was performed on the samples. The BET surface area of the mesoporous transparent film and scattering film were 85 $m^2\ g^{-1}$ and 27 $m^2\ g^{-1}$. The values of the two films porosity were 70% and 65% for transparent film and scattering film respectively. Prior to dye loading, photoanodes were sintered again at 480 °C for 30 minutes. Afterward, substrate was cooled down to 80 °C and immersed in the dye solutions for overnight. After rinsing with the acetonitrile, the stained substrates were sealed with pieces of thermally platinized electrode. The platinized electrode was made using a solution of H_2PtCl_6 on FTO glass (TEC15, Pilkington), and served as a counter electrode. The working and counter

electrodes were separated by 25 μm-thick hot melt ring (Surlyn, DuPont) and sealed by heating. The electrolytes were introduced to the cells via pre-drilled holes in the counter electrodes.

Photovoltaic characterization. The setup used for standard photovoltaic characterization (J–V curve) consisted of a 450 W Xenon lamp (Oriel), whose spectral output was matched in the region of 350–750 nm with the aid of a Schott K113 Tempax sunlight filter (Präzisions Glas & Optik GmbH), and a source meter (Keithley 2400) to apply potential bias and measure the photocurrent. A set of metal mesh filters was used to adjust the light intensity to a desired level. A black metal mask defined the cell active area to be 0.158 cm^2.

Preparation of dyes and electrolytes. Dyes and electrolyte composition are as following: Z907 dye solution: Z907 dye (0.3 mmol concentration) is dissolved in tert- butanol/ acetonitrile (ACN) solvent mixture (1:1 v/v). Y123 dye solution: Y123 dye dissolved in a 0.1-mmol dye solution in a tert- butanol/ acetonitrile mixture (1:1 v/v). Iodide based electrolyte coded Z946: I_3^-/I^- based electrolyte in 3-methoxypropionitrile (MPN) as solvent. 1.0 M DMII, 0.15 M I2, 0.5 M NBB, and 0.1 M GNCS in MPN. Cobalt based electrolyte coded Z1148: Co (II)/Co (III) based redox electrolyte in acetonitrile as solvent. 0.22M $Co^{II}(Bpy)_3(B(CN)_4)_2$,0.033M $Co^{III}(Bpy)_3(B(CN)_4)_3$, 0.1M $LiClO_4$, 0.2M TBP in ACN.

References

1. Yella, A. *et al.* Porphyrin-sensitized solar cells with cobalt (II/III)-based redox electrolyte exceed 12 percent efficiency. *Science* **334,** 629–634 (2011).
2. Moser, J.-E. Dynamics of interfacial and surface electron transfer processes in *Dye-Sensitized Solar Cells* (ed. Kalyanasundaram, K.) Ch. 11, 403–456 (EPFL Press, Lausanne, 2010).
3. Haque, S. A. *et al.* Charge separation versus recombination in dye-sensitized nanocrystalline solar cells: The minimization of kinetic redundancy. *J. Am. Chem. Soc.* **127,** 3456–3462 (2005).
4. Teuscher, J. *et al.* Photoinduced interfacial electron injection dynamics in dye-sensitized solar cells under photovoltaic operating conditions. *J. Phys. Chem. Lett.* **3,** 3786–3790 (2012).
5. Juozapavicius, M., Kaucikas, M., van Thor, J. J. & O'Regan, B. C. Observation of multiexponential pico- to subnanosecond electron injection in optimized dye-sensitized solar cells with visible-pump mid-infrared-probe transient absorption spectroscopy. *J. Phys. Chem. C* **117,** 116−123 (2013).
6. Antila, L. J., Myllyperkiö, P., Mustalahti, S., Lehtivuori, H., Korppi-Tommola, J. Injection and ultrafast regeneration in dye-sensitized solar cells. *J. Phys. Chem. C* **118,** 7772−7780 (2014).
7. Brauer, J. C., Marchioro, A., Paraecattil, A. A., Oskouei, A. & Moser, J.-E. Dynamics of interfacial charge transfer states and carriers separation in dye-sensitized solar cells: A time-resolved terahertz spectroscopy study. *J. Phys. Chem. C* **119,** 26266–26274 (2015).
8. Ito, S. *et al.* Fabrication of thin film dye-sensitized solar cells with solar to electric power conversion efficiency over 10%. *Thin Solid Films* **516,** 4613–4619 (2008).
9. Kessler, R. W. & Wilkinson, F. Diffuse reflectance triplet–triplet absorption spectroscopy of aromatic hydrocarbons chemisorbed on γ-alumina. *J. Chem. Soc., Faraday Trans. 1* **77,** 309–320 (1981).
10. Colombo, D. P. & Bowman, R. M. Femtosecond diffuse reflectance spectroscopy of TiO_2 powders. *J. Phys. Chem.* **99,** 11752–11756 (1995).
11. Asahi, T., Matsuo, Y. & Masuhara, H. Localization of a charge transfer excited state in molecular crystals: A direct confirmation by femtosecond diffuse reflectance spectroscopy. *Chem. Phys. Lett*. **256,** 525–530 (1996).
12. Fukumura, H., Ichikawa, M. & Masuhara, H. Development of a femtosecond diffuse reflectance spectroscopic system, evaluation of its temporal resolution, and applications to organic powder systems. *Rev. Sci. Instrum.* **9,** 369–371 (1998).
13. Furube, A. *et al.* Femtosecond diffuse reflectance transient absorption for dye-sensitized solar cells under operational conditions: effect of electrolyte on electron injection. *J. Am. Chem. Soc.* **132,** 6614–6615 (2010).
14. Mohammadpour, R., Iraji zad, A., Hagfeldt, A. & Boschloo, G. Comparison of trap-state distribution and carrier transport in nanotubular and nanoparticulate TiO_2 electrodes for dye-sensitized solar cells. *Chemphyschem* **11,** 2140–2145 (2010).
15. Shankar, K. *et al.* Highly efficient solar cells using TiO_2 nanotube arrays sensitized with a donor-antenna dye. *Nano Lett.* **8,** 1654–1659 (2008).
16. Ghadiri, E., Taghavinia, N., Zakeeruddin, S. M., Grätzel, M. & Moser, J.-E. Enhanced electron collection efficiency in dye-sensitized solar cells based on nanostructured TiO_2 hollow fibers. *Nano Lett.* **10,** 1632–1638 (2010).
17. Ghadiri, E., Taghavinia, N. & Aghabozorg, H. R. TiO_2 nanotubular fibers sensitized with CdS nanoparticles. *The European Physical Journal Applied Physics*. **50(02),** 20601 (2010).
18. Ito, S. *et al.* Study of dye-densitized solar cells by scanning electron micrograph observation and thickness optimization of porous TiO_2 electrodes. *Int. J. Photoenergy.* **2009,** 1–8 (2009).
19. Wang, P. *et al.* A stable quasi-solid-state dye-sensitized solar cell with an amphiphilic ruthenium sensitizer and polymer gel electrolyte. *Nat. Mater.* **2,** 402–407 (2003).
20. Ito, S. *et al.* Bifacial dye-sensitized solar cells based on an ionic liquid electrolyte. *Nat. Photonics.* **2,** 693–698 (2008).
21. Tsao, H. N. *et al.* Cyclopentadithiophene bridged donor–acceptor dyes achieve high power conversion efficiencies in dye-sensitized solar cells based on the tris-cobalt bipyridine redox couple. *ChemSusChem* **4,** 591–594 (2011).
22. Yum, J.-H. *et al.* A cobalt complex redox shuttle for dye-sensitized solar cells with high open-circuit potentials. *Nat. Commun.* **3,** 631 (2012).
23. Marchioro, A., Dualeh, A., Punzi, A., Grätzel, M. & Moser, J.-E. Effect of posttreatment of titania mesoscopic films by $TiCl_4$ in solid-state dye-sensitized solar cells: a time-resolved spectroscopy study. *J. Phys. Chem. C* **116,** 26721–26727 (2012).
24. Katoh, R. & Furube, A. Efficiency of electron injection in dye-sensitized semiconductor films. *Key Engineering Materials* **451,** 79–95 (2011).
25. Katoh, R., Yaguchi, K. & Furube, A. Effect of dye concentration on electron injection efficiency in nanocrystalline TiO_2 films sensitized with N719 dye. *Chem. Phys. Lett.* **511,** 336–339 (2011).
26. Katoh, R., Tamaki, Y. & Furube, A. Primary photocatalytic reactions in TiO_2 nanoparticles studied by time-resolved laser spectroscopy. *Proc. SPIE.* 8109, 81090–81098 (2011).
27. Colombo, P., Jr. *et al.* Femtosecond study of the intensity dependence of electron-hole dynamics in TiO_2 nanoclusters. *Chem. Phys. Lett.* **232,** 207–214 (1995).
28. Bräm, O., Cannizzo, A. & Chergui, M. Ultrafast fluorescence studies of dye-sensitized solar cells. *Phys. Chem. Chem. Phys.* **14,** 7934–7937 (2012).
29. Wenger, B., Grätzel, M. & Moser, J.-E. Rationale for kinetic heterogeneity of ultrafast light-induced electron transfer from Ru(II) complex sensitizers to nanocrystalline TiO_2. *J. Am. Chem. Soc.* **127,** 12150–12151 (2005).

30. Benkö, G., Kallioinen, J., Korppi-Tommola, J. E. I., Yartsev, A. P. & Sundström, V. Photoinduced ultrafast dye-to-semiconductor electron injection from nonthermalized and thermalized donor states. *J. Am. Chem. Soc.* **124,** 489–493 (2002).
31. O'Regan, B. C. *et al.* Measuring charge transport from transient photovoltage rise times. A new tool to investigate electron transport in nanoparticle films. *J. Phys. Chem. B* **110,** 17155–17160 (2006).
32. Sá, J. *et al.* Transient mid-IR study of electron dynamics in TiO_2 conduction band. *Analyst* **138,** 1966 (2013).
33. Xiong, W. *et al.* Transient 2D IR spectroscopy of charge injection in dye-sensitized nanocrystalline thin films. *J. Am. Chem. Soc.* **131,** 18040–18041 (2009).
34. Richter, C. & Schmuttenmaer, C. A. Exciton-like trap states limit electron mobility in TiO_2 nanotubes. *Nat. Nanotechnol.* **5,** 769–772 (2010).
35. Wang, L. *et al.* Universal electron injection dynamics at nanointerfaces. *Adv. Funct. Mater.* **22,** 2783–2791 (2012).
36. Feldt, S. M. *et al.* Design of organic dyes and cobalt polypyridine redox mediators for high-efficiency dye-sensitized solar cells. *J. Am. Chem. Soc.* **132,** 16714–16724 (2010).
37. Cappel, U. B., Feldt, S. M., Schöneboom, J., Hagfeldt, A. & Boschloo, G. The influence of local electric fields on photoinduced absorption in dye-sensitized solar cells. *J. Am. Chem. Soc.* **132,** 9096–9101 (2010).
38. Xu, M. *et al.* Joint electrical, photophysical and computational studies on D-π-A dye-sensitized solar cells: the impacts of dithiophene rigidification. *Chem. Sci.* **3,** 976 (2012).
39. Ghadiri, E. Time-resolved diffuse reflectance spectroscopy of efficient dye- and semiconductor-sensitized solar cells under operational conditions. PhD thesis, *École Polytechnique Fédérale de Lausanne* (2014).
40. Kubelka, P. & Munk, Z. Z. Ein Beitrag Zur Optik Der Farbanstriche. *Ann. Techn. Phys* **11,** 593–601 (1931).
41. Kortum, G. *Reflectance Spectroscopy*, *Principles And Applications*. (Springer-Verlag, New York, 1969).

Acknowledgements

We thank R. Humphry-Baker, M. Chergui and T. Moehl for fruitful discussions. P. Comte for the preparation of standard TiO_2 photoanodes, J. -D. Décoppet for I-V measurement and R. Mohammadpour for kindly providing TiO_2 anodized nanotube films. Financial support by NCCR MUST, an instrument of the Swiss National Science Foundation, is gratefully acknowledged.

Author Contributions

E.G. designed and developed the femtosecond diffuse reflectance spectrometer, fabricated devices, carried out experiments, analyzed results, and wrote the paper. S.M.Z. provided dyes and electrolytes, contributed to discussions, and revised the paper. A.H. and M.G. contributed to the discussions and interpretation of data and revised the paper. J.-E.M. designed the research project, directed the experiments, and contributed to the interpretation of data, and revised the manuscript.

Additional Information

Supplementary information accompanies this paper at http://www.nature.com/srep

Competing financial interests: The authors declare no competing financial interests.

How to cite this article: Ghadiri, E. *et al.* Ultrafast charge separation dynamics in opaque, operational dye-sensitized solar cells revealed by femtosecond diffuse reflectance spectroscopy. *Sci. Rep.* **6**, 24465; doi: 10.1038/srep24465 (2016).

SUPPLEMENTARY INFORMATION

Ultrafast charge separation dynamics in opaque, operational dye-sensitized solar cells revealed by femtosecond diffuse reflectance spectroscopy

Elham Ghadiri[1*], Shaik M. Zakeeruddin[2], Anders Hagfeldt[3], Michael Grätzel[2], and Jacques-E. Moser[1]

1 Photochemical Dynamics Group, 2 Laboratory for Photonics and Interfaces and 3 Laboratory of Photomolecular Science**,** Institute of Chemical Sciences and Engineering, Ecole Polytechnique Fédérale de Lausanne, CH-1015 Lausanne Switzerland

E-mail address: Elham.ghadiri@alumni.epfl.ch

1. Time-resolved diffuse reflectance spectroscopy

State of the art pump-probe diffuse reflectance spectrometer

Figure S1 depicts the schematic of developed femtosecond time-resolved diffuse reflectance spectrometer. The new design of light collection configuration based on coupled off-axis parabolic mirrors allowed us to achieve a time resolution of sub-200 fs and collection of light with a big solid angle. The technique enables, the study of opaque solid films as well as highly absorbing systems.

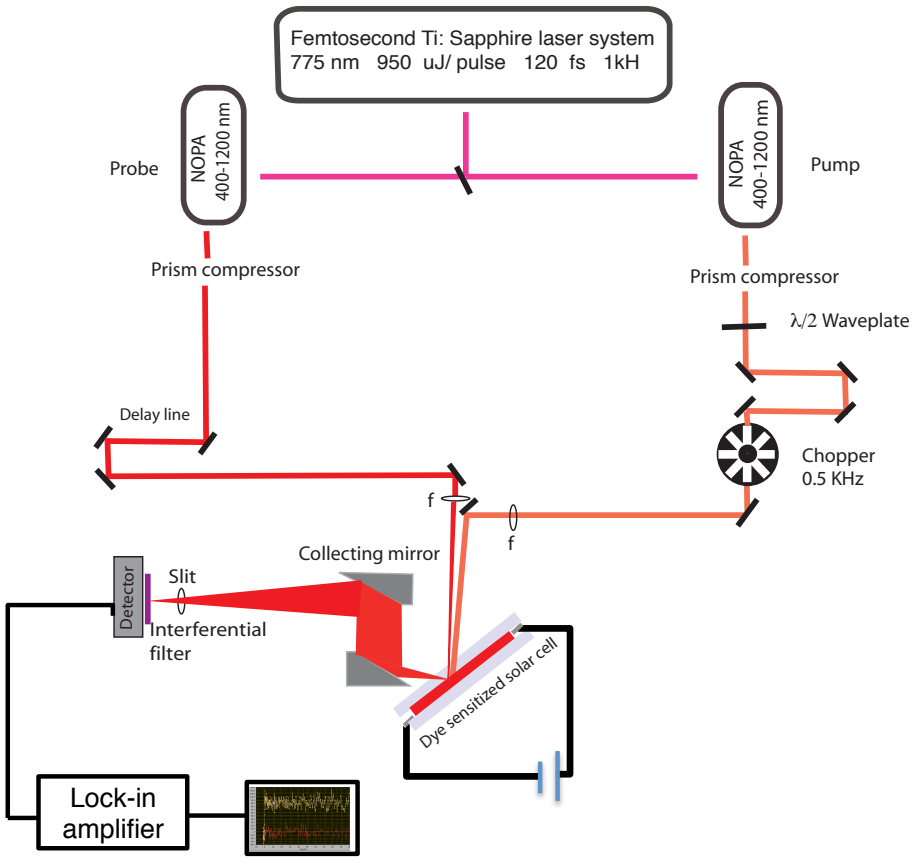

Figure S1. Schematic of designed and developed femtosecond time-resolved diffuse reflectance spectrometer. Setup is composed of a femtosecond laser, double stage non-collinear optical parametric amplifier (NOPA), parabolic light collecting mirrors, diode detector, and lock-in amplifier. The sample is a DSC device biased under working potential.

Quantitative data analysis and optical modeling

Figure S2 shows the pump-probe diffuse reflectance signal at a delay time of 50 ps as a function of excitation intensity. The amplitude of the signal shows a good linear response to the excitation intensity tuned over a wide range.

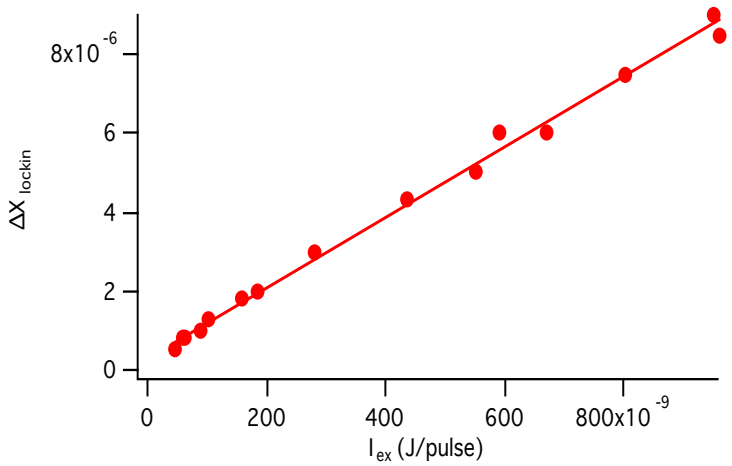

Figure S2. Linearity test. Transient diffuse reflectance measurements over a broad excitation pulse energy range are shown. The sample is a dye-sensitized double layer TiO_2 film. The pump beam energy is changed from 0.047 µJ to 0.95 µJ. The y-axis is the amplitude of the pump-probe signal at 50 ps after pulse excitation. The amplitude of the signal versus the excitation intensity shows a linear behavior.

The Kubelka-Munk formalism is applied to the time-resolved diffuse reflectance measurements according to equation (3) of the main text. The Kubelka-Munk function, which is representative of the concentration of absorbing species in the film, shows a perfect linear response over the excitation energy of pump beam.

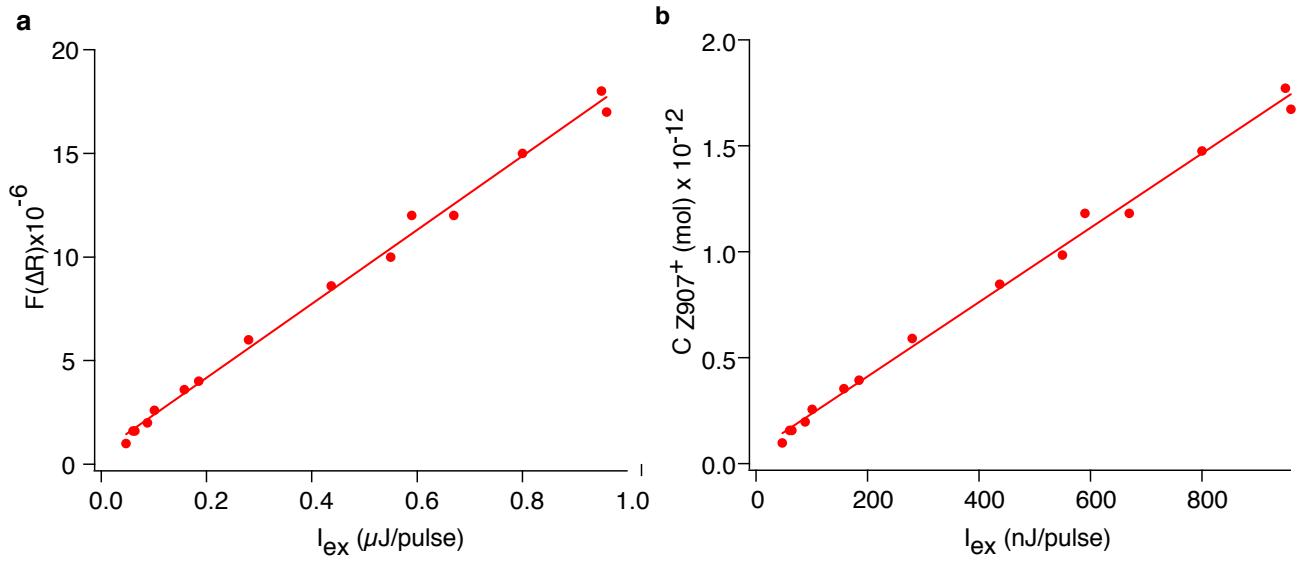

Figure S3. Quantitative analysis of diffuse reflectance measurements. The evolution of the transient Kubelka-Munk function upon an increase in excitation pulse energies are shown. The Kubelka- Munk function is integrated on the transient diffuse reflectance at a wavelength of 840 nm, measured on DSC based on Z907 sensitized double layer TiO_2 film. b) Extracted concentration of oxidized dye molecules at different excitation pulse energies deduced from Kubelka- Munk formalism. At a broad energy scale of pulse excitation, the obtained Kubelka-Munk function and consequently concentration of transient species show a linear trend.

2. Kinetics studies

Influence of excitation intensity on the kinetics in Z907 sensitized complete photoanode

Intensity dependence of diffuse reflectance measurements on Z907 sensitized complete DSC photoanode (double layer) in the presence of MPN solvent is presented in Figure S4. The signals can be fitted with single exponential function. The observed kinetics at 840 nm is assigned to the early back recombination of photoinjected electrons with oxidized dye molecules. It should be noted that in kinetics studies all the measurements are performed at very low excitation intensities (below 300 nJ/ pulse).

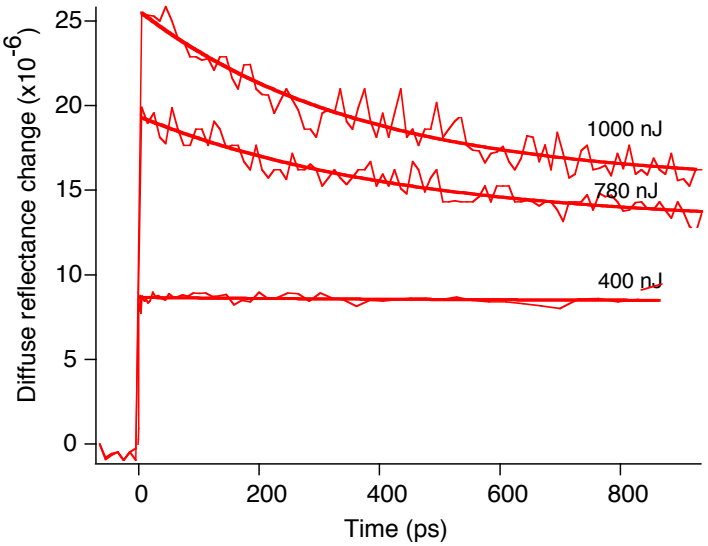

Figure S4. Excitation intensity dependence test. Transient diffuse reflectance measurements on Z907 sensitized TiO_2 double layer film immersed in MPN solvent at different excitation intensities. The probe beam wavelength is 840 nm. At the excitation of 1000 nJ, the kinetics is fitted with a double exponential. Excitation pulse energy is changed by one order of magnitude from 300 nJ to 1000 nJ. Consequently, the amplitude of the signal is raised, and the decay kinetics is accelerated. Rate constants of single exponential decay function fit to traces measured at 400 nJ, 780 nJ, and 1000 nJ are respectively, 0.0014×10^{12} s^{-1}, 0.0023×10^{12} s^{-1} and 0.0028×10^{12} s^{-1}. This depleting kinetics represents an early back reaction of electrons with oxidized molecules.

Effect of probe wavelength

The evolution of oxidized dye molecule is also probed in the visible wavelength region at 670 nm and is compared with the measurements at 840 nm. The early back recombination kinetics is again observed when the diffuse reflectance measurements kinetics is recorded at 670 nm. The signal is fitted with single exponential function. The first order rate constant for measurement at 670 nm is 0.0008 $\times 10^{12}$ s^{-1} that corresponds to a time constant of 1.25 ns. Excitation intensity is 400 nJ/pulse.

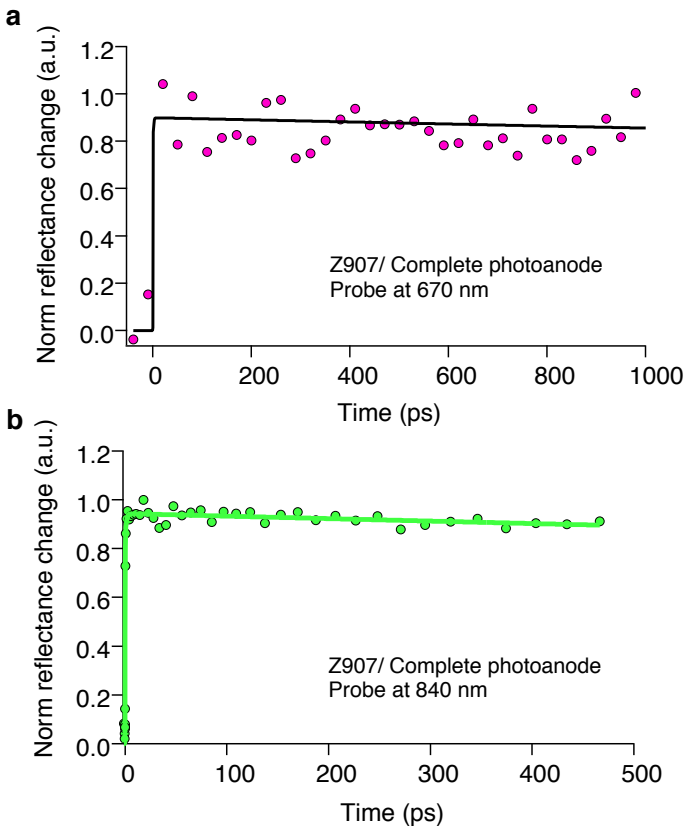

Figure S5. Kinetics monitored at different probe wavelength. Normalized diffuse reflectance change of Z907 sensitized double layer film recorded at 670 nm and 840 nm. The first order rate constant for measurement at 670 nm is $0.0008 \times 10^{12}\ s^{-1}$ that corresponds to a time constant of 1.25 ns. Excitation intensity is 400 nJ/pulse. The trace b is identical to the Figure 2c of the main text and is depicted here for comparison.

Effect of TiO_2 film morphology and presence of electrolyte

To understand the effect of morphology on the kinetics of charge separation process, we also investigated the electron injection profiles in DSC devices based on different opaque nanostructured TiO_2 films like TiO_2 nanofibers, and TiO_2 nanotubes prepared by anodization of Ti foil. Figure 4-9 shows the dynamics of electron injection on Z907 dye-sensitized TiO_2 of various morphologies monitored at 840 nm. Panel a shows the kinetics of charge separation in Z907 dye-sensitized standard double layered based DSC device in the presence and absence of redox electrolyte. Similar measurement on Z907 dye-sensitized anodized TiO_2 nanotubes film in the presence of MPN solvent and redox electrolyte is also presented. It is interesting to observe that the electron injection is still in the ultrafast regime, and the recombination features are still present. It should be noted that the picosecond recombination feature is occurring in nanotubes with different relative amplitude compared to that of scattering particles.

Transient absorption studies on the band gap excitation of bare TiO_2 nanocrystalline films is performed by Furube and co-workers[1]. They have observed that after ultrafast formation of electron hole in TiO_2 particles, the surface trap electrons and surface trap holes forms in 200 fs (in the limit of time resolution) and relax to deep bulk traps in 500 ps. However, our measurements situation is slightly different with those studies in the sense that our samples are dye-sensitized TiO_2 films. In our system, the electrons are in the TiO_2 particles and holes are in the oxidized dye molecules. Although the photoinjected electrons can trap, in the same way, as what was observed for bare TiO_2 particles by groups of Colombo and Furube[1,2].

In anodized TiO_2 nanotube film, the trap states are energetically deeper than in the TiO_2 nanoparticle film as it was measured previously by modulated voltage-current techniques and terahertz spectroscopy[3,4]. So, the trap state distribution difference could play a vital role in decreasing the observed decreased relative amplitude of the picosecond recombination feature (i.e. the loss of electrons due to back recombination) in the study with nanotubes compared to nanoparticle film (black and green traces in 4a and 4b). Therefore, in nanotubes films, electrons that are trapped in the films are less free to undergo the early picosecond recombination in comparison to what is seen in particles.

Modeling of the laser induced photovoltage in the solar cell and dark current correction

In this model, a chemical capacitance is assigned to the DSC. The capacitance of the cell is measured by impedance spectroscopy, at each bias voltage. The chemical capacitance in the TiO_2 film increases (as the applied forward bias is increased). The amount of photoinjected charge into this capacitor is estimated based on quantification of the transient diffuse reflectance spectrum. Kubelka-Munk formalism is integrated on the diffuse reflectance spectrum, as it is proportional to the concentration of absorbing species.

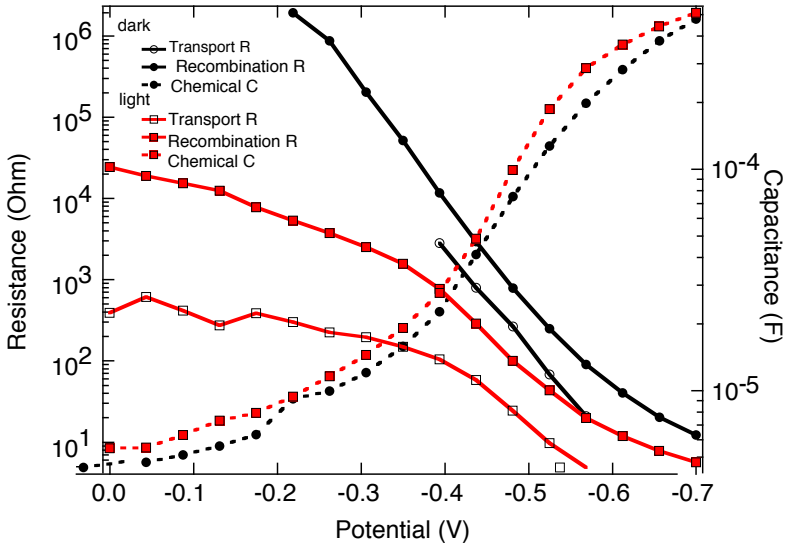

Figure S6. Impedance spectroscopy. Impedance measurements on DSC based on Z907 dye and Z946 electrolyte. The cell active area is 0.283 cm^2.

Having:

$$\Delta Q = C\Delta V \quad \text{(S1)}$$

$$\Delta Q_{Pulse} \cong C^{+}_{Z907} \quad \text{(S2)}$$

The photovoltage induced by each laser pulse is estimated to be about 10 μV at 700 mV bias voltage and 38 μV when the cell is biased at 520 mV. However for laser spectroscopy measurements on the cell at short circuit condition or small bias voltage, the amount of laser induce shift in the quasi-Fermi level position is in the order of some mV.

A good approximation of dark current correction is to consider the cell series resistance and according to Ohm law draw the voltage drop in the cell due to dark current.

$$\Delta V_{Voltage\ drop} \cong R_{Series} I_{dark} \quad \text{(S3)}$$

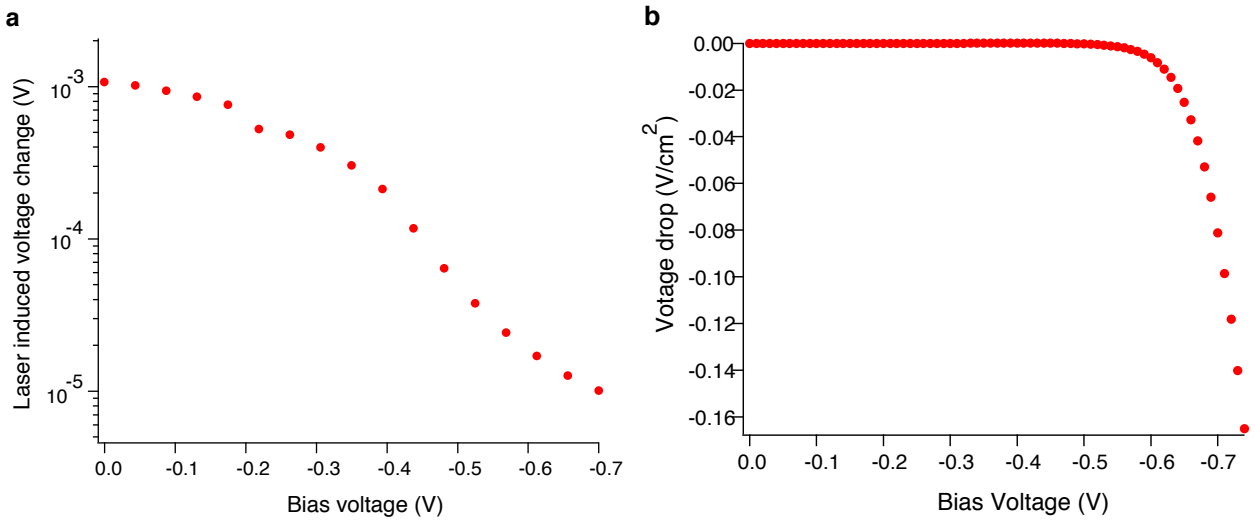

Figure S7. Laser induced voltage rise and voltage drop due to dark current in DSC. a) The amount of laser pulse induces change in the voltage of the solar cell when the pump-probe experiments are performed on the solar cell under operational condition is calculated. The amount of laser induced voltage raise compared to the applied bias voltage is negligible. b) The voltage drop at the cell filled by active layer mainly due to dark current at different bias voltages. The voltage drop is estimated from Ohm law and the measured series resistance in the solar cell device. The I-V curve of the device is shown in figure 5a of the main text.

Comparison of the photovoltaic and optical response of two different DSC devices made based on transparent layer, and scattering layer film of same thickness

Two types of DSC devices based on two different TiO_2 films with same thickness sensitized with Z907 dye were made. The first device is based on a 5 µm-thick TiO_2 film made of scattering particles and the second device is made of a 5 µm-thick transparent TiO_2 layer. All preparation and test situation were identical for both devices. The morphological parameters, optical properties and photovoltaic performances of the devices are depicted in Table S1.

As depicted in Table S1, in the scattering TiO_2 layer, the BET surface area is 27 m^2/gr and the roughness factor of the film is 36.4 /cm^2 µm. These values are much smaller than those in transparent layer film being 85 m^2/gr and 98 /cm^2 µm respectively. Therefore a smaller amount of dye is adsorbed on the scattering layer film. Therefore, the value of the maximum light absorptance ($\mathcal{A}$) in the scattering layer is 0.66 and is smaller than that in the transparent film being 0.88. The photocurrent generated in a DSC device made of transparent layer is 11.4 mA/cm^2 while this value for scattering TiO_2 layer based device is only 5.9 mA/cm^2. The difference in the photocurrent is due to the amount of adsorbed dye molecule in the two films. For a fair comparison, the photocurrent of

devices is normalized to the absorptance of the film. The obtained value for the transparent layer is 12.95 while for scattering layer is only 8.93. Therefore, the amount of J/ $\mathcal{A}$ (current normalized to the absorptance) for the scattering film is 30% less than that of the transparent layer. This observation indicates that in the scattering layer based device about 30% of the photo-generated electrons are lost. This can be in agreement with our laser spectroscopy results that for big particles we witnessed loss of electrons due to prompt back recombination.

Table S1. Comparison of the structural, optical and photovoltaic properties of two DSC devices based on scattering layer and transparent layer of identical thickness.

TiO_2 film	Film roughness factor (cm^{-2} μm^{-1})	BET Surface area (m^2/gr)	Absorptance ($\mathcal{A}$)	Jsc (mA)	Jcs/ $\mathcal{A}$ (mA)	Voc (mV)
Scattering layer (5 μm)	36.4	27	0.66	5.9	8.93	704.9
Transparent layer (5 μm)	98	85	0.88	11.4	12.95	697.6

3. Electron injection in Y123 dye-sensitized solar cell devices

Figure S8 illustrates the steady-state absorbance spectrum of Y123 dye measured in solution. The first absorption peak of the dye is at 530 spectral regions.

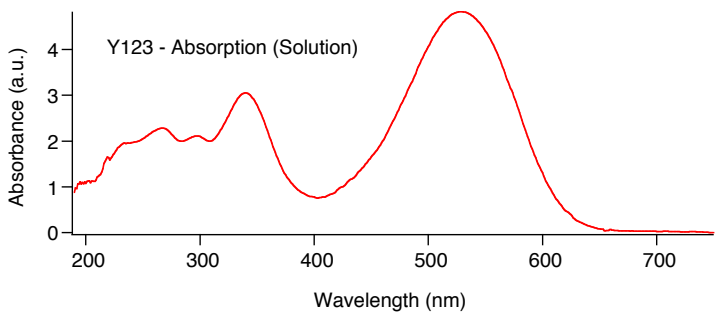

Figure S8. Optical analysis. Steady-state absorbance spectrum of the Y123 dye in solution.

Effect of liquid environment

Figure S9 depicts the measurements on Y123 dye-sensitized different TiO_2 films in the presence of only MPN solvent probed at 840 nm. Comparing with the measurements in the presence of the electrolyte, which is shown in figure 6 of the main text, no obvious difference is observed, and the kinetics are independent of the environment.

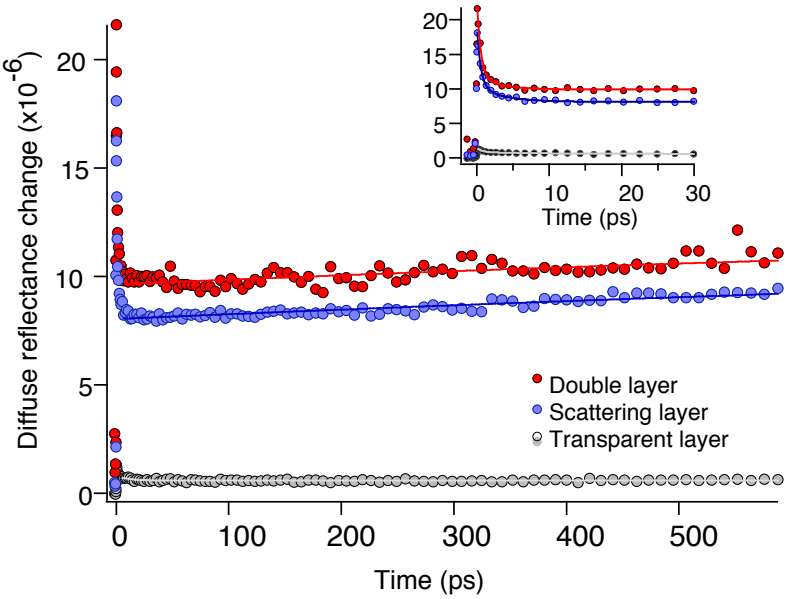

Figure S9. Femtosecond diffuse reflectance measurements on Y123 dye-sensitized TiO_2 films in the presence of MPN solvent. Red markers (double layer), blue markers (scattering layer) and gray markers (transparent layer). The time constants of the exponential fit to the decay component of the signals are: τ_1= 7.249 ps and τ_2= 0.663 ps for the transparent film, τ_1= 3.623 ps and τ_2= 0.552 ps for the scattering film and τ_1= 3.116 ps and τ_2= 0.553 ps for the double layer film.

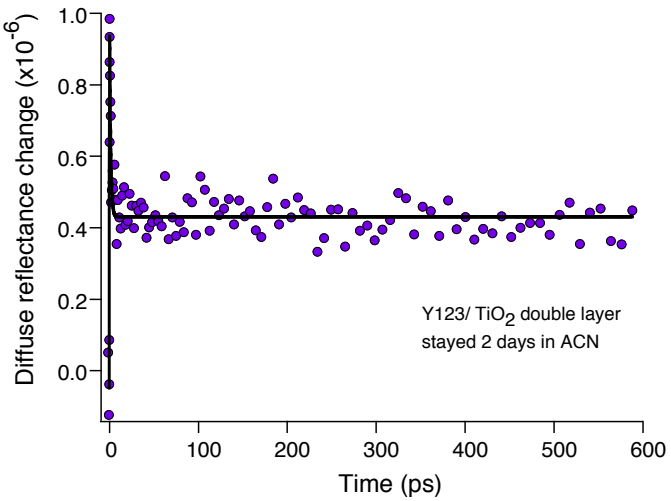

Figure S10. Effect of acetonitrile treatment. Femtosecond diffuse reflectance measurement on organic Y123 dye-sensitized TiO_2 double layer film immersed two days in acetonitrile after dye loading.

Figure S10 shows the measurements on double layer film immersed for two days in acetonitrile, which is the same sample for which the kinetics is shown in the red trace in figure 6 of the main text. We observe that after immersing in acetonitrile, the slow rise kinetics is removed, and a flat kinetics is replaced. This is due to dissolving of the extra dye molecules attached to the surface of the film in the form of dye aggregates.

Figure S11a shows the transient absorbance spectrum of the Y123 dye in solution. The pump excitation wavelength in these measurements is 600 nm. A negative peak around 520 nm is observed which can be assigned to the bleaching of the ground state absorption of the dye upon photo-excitation. This peak is consistent with the optical absorption peak of the dye in figure S8. The recovery of the ground state bleaching of the dye is fast. This kinetics can be fitted with a single exponential function indicating a time constant of 57 picoseconds. A positive peak is observed in the wavelength region from 630 nm to 680 nm. The small positive feature in the spectrum around 565 nm can be a tail of the same absorption feature, which is partially, covered by laser pulse excitation at 600 nm. The positive peak can be assigned to the excited state absorption of the Y123 dye. This deactivation of the Y123 dye excited state can be fitted to a single exponential function with almost the same lifetime of about 50 ps and, therefore, has a mirror-like kinetics to ground state bleaching. A small negative peak at the NIR region about 750 nm is assigned to the emission of the dye.

Figure S11b shows the spectrum of the transient absorbance change of the dye anchored on TiO_2 films. It is observed that negative peak at 500 nm that is assigned to the ground state bleaching, when the dye is anchored onto TiO_2 surface, is very small and a clear red-shift in the bleaching of the ground state absorption of about 60 nm is observed. Although this red-shifted pick is overlapped and partially covered with the excitation beam at 600 nm, it is clearly resolved. This red- shift in the transient absorption spectrum of the dye molecule is probably an evidence for Stark-shift of the ground state absorption of the dye molecule. The Stark-shift effect was previously observed in other organic dyes by Boschloo et al. and in Ru-based dyes by Meyer and co-workers. This observation is explained by the shift of ground state absorption of the dye molecule, which is influenced, from the

local electric field induced by the electric dipole of the neighbor dye molecules. Finally, the positive feature above 630 nm in solid sample is now assigned to a contribution of both of the excited state absorption of the dye and the absorption by oxidized dye molecule formed upon injection of electrons into TiO_2 conduction band.

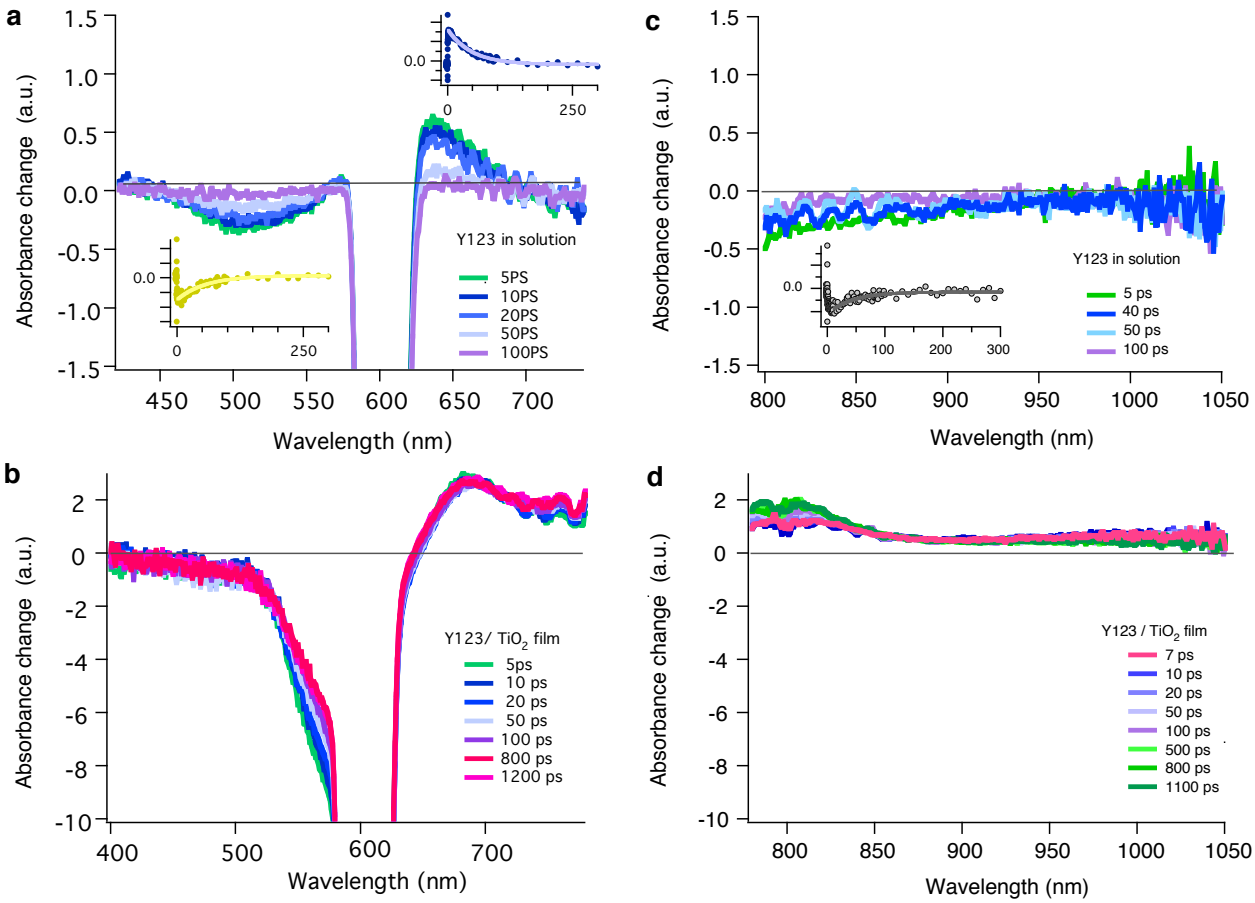

Figure S11. Transient white light continuum spectrum. a) Y123 dye measured in solution and b) Y123 sensitized TiO_2 transparent film, in the visible light wavelength region. The pump excitation is at wavelength 600 nm. c,d) NIR transient white light continuum spectrum of c) Y123 dye measured in solution and d) Y123 sensitized TiO_2 transparent film, in NIR wavelength region. The excitation wavelength is at wavelength 600 nm. Excitation intensities are 300 nJ/ pulse for films and 1000 nJ/ pulse for measurement in solution.

Figure S11c and S11d depict the NIR transient absorbance spectrum of the Y123 dye in solution and anchored on TiO_2 film. The excitation wavelength at these measurements is 600 nm. In the transient spectrum of the dye in solution, the negative peak at NIR region up to 950 nm can be due to the emission of the dye. The spectrum of the Y123 sensitized TiO_2 film shows a contribution of both absorption of oxidized dye molecules and dye emission.

References:

1. Tamaki, Y. et al. Dynamics of efficient electron-hole separation in TiO_2 nanoparticles revealed by femtosecond transient absorption spectroscopy under the weak-excitation condition. *Phys. Chem. Chem. Phys.* **9**, 1453 (2007).
2. Colombo, D. P. & Bowman, R. M. Femtosecond diffuse reflectance spectroscopy of TiO_2 powders. *J. Phys. Chem.* **99**, 11752–11756 (1995).
3. Mohammadpour, R., Iraji zad, A., Hagfeldt, A. & Boschloo, G. Comparison of Trap-state Distribution and Carrier Transport in Nanotubular and Nanoparticulate TiO_2 Electrodes for Dye-Sensitized Solar Cells. *Chemphyschem* **11**, 2140–2145 (2010).
4. Richter, C. & Schmuttenmaer, C. A. Exciton-like trap states limit electron mobility in TiO_2 nanotubes. *Nat Nanotechnol* **5**, 769–772 (2010).